BIOLOGICALLY INSPIRED
ROBOTICS GROUP (BIRG)

Analysis of hydrodynamic forces on the model of a swimming salamander

Anurag Tripathi,
Department of Mechanical Engineering,
Indian Institute of Technology,
Kanpur.

July 12, 2003

Contents

1 Introduction

Locomotion is one of the primary characteristics of animals which separates them from plants. Locomotion enables animals to find their food and to move from one place to another. This importance of locomotion makes it extremely important to study various mechanisms underlying locomotion. A study of these mechanisms can help tremendously to develop robots which can locomote in the same way as animals do. Amphibians are vertebrates which can swim in water as well as walk on ground. The salamander is an amphibian of great interest to the neurobiologists for studying the mechanisms which aid in locomotion. The importance of the salamander arises due to the fact that it is one of the most primitive creatures which made transition from swimming to walking. Therefore, the study of mechanisms responsible for the swimming and walking of salamander can provide useful information which could be used for developing robots which can swim as well as walk on ground. Moreover, the salamander has a simple body framework which facilitates an easier fabrication of a model similar to the actual salamander. At the same time, the mechanisms are adequately complex to get a detailed information about the movement patterns in many similar creatures. The aim of this report is to investigate the hydrodynamic forces on a salamander model and to ascertain various factors which affect the swimming of salamander model. The model was subjected to different kinds of forces and a detailed study of the swimming motion of salamander model will be presented in the following sections of this report.

2 Mechanical simulation of the salamander

The salamander model used for analysis had the dimensions of a salamander robot currently under construction; to be used for experimentation in near future. The mechanical model of salamander consisted of a 70 cm long body which was made up of 10 rigid links representing the trunk and the tail. The links were connected by one-degree-of-freedom hinge joints. The length of each link was 7 cm and each link had a rectangular cross section of 3.5 cm width and 5.5 cm height. The density of salamander model was assumed to be equal to that of water (i.e.1000 kg/m^3). The model was approximately three times bigger than most salamander species as this study is supposed to be used for the design of robots which could locomote like a salamander on the provision of necessary input. The salamanders are very small in size whereas the model was made keeping in mind the dimensions of the robot whose swimming motion will be compared with the results of this report.

The model was implemented with the help of *ODE* (Open Dynamics Engine) software which is very useful for the dynamic simulations of articulated rigid bodies. Alessandro Crespi of the Biologically Inspired Robotics Group at the Logic Systems Laboratory, EPFL developed the code for generating the salamander model. I applied hydrodynamic forces on the model and analysed its response to these forces. A swimming salamander is subjected to inertial as well as the viscous forces which will be discussed in the next section of this report. This project was undertaken with the view to realize certain goals.

1. To invoke maximum possible realism in experimental simulation by using the results of this analysis.

2. To make predictions about the behaviour of salamander robot subject to hydrodynamic forces.

3. To help designing the robot by finding out the number of body links and the size of limbs which aid in proper swimming of the salamander robot.

4. To check the supposition that it is inertial forces which play a major role in the swimming of salamander model at high swimming speeds.

Keeping these objective in mind, certain schemes were developed which suggested the formulations for inertial and viscous forces and the model was subjected to forces calculated from these formulations. First, the motion of salamander model was studied for forces in 2-D and the study was then extended to the scheme in which the model was subjected to forces in 3-D.

3 Concept of inertial and viscous forces

When there is relative motion between a solid object and a fluid, certain forces come into play which retard the relative motion between solid and fluid. These forces are termed as drag forces. There are two kind of drag forces: Inertial and Viscous.

1. Inertial Drag: It is the resistance to relative motion caused by inertia i.e the tendency of a particle may it be solid or fluid, to remain in its state of rest or of uniform motion. If a solid object moves through a fluid, it disturbs the state of rest of surrounding fluid particles which in turn exert normal resistive forces on the solid surface which retard the motion of solid through the fluid medium.

2. Viscous Drag: It is the resistance to relative motion caused by no slipping condition at the solid-liquid interface. No slipping implies that the relative speed at solid-liquid interface is zero. All real fluids satisfy no slipping condition at the solid-liquid interface. When a solid object advances through a fluid, it tends to carry the fluid particles at the surface along with it whereas the fluid particles tend to retard the motion of solid object. This results into the development of shear stress at the solid-liquid interface which retards the moving object and acts tangentially on the solid surface, resulting into viscous drag.

Formulations for inertial and viscous forces will be discussed later in this report.

4 Analysis of salamander model under the influence of forces in 2-D

This section investigates the magnitude of inertial forces versus viscous forces to ascertain their influence over the motion of salamander model. We dealt with the problem initially in 2-D as the biological salamander exhibits planar swimming. Planar swimming implies that the general swimming pattern of a salamander can be considered as the movement in a plane in a particular direction and that there is no movement of the center of mass of salamander in the direction normal to that plane. The attributes of planar swimming in the salamander model were included through the inclusion of hinge joints between consecutive links. Thus, by construction, all the undulations were in a plane as all hinges had their axis of rotation aligned. But the plane in which undulations were taking place had the freedom to rotate upon the application of external moments or forces. Analysis of the model in 3-D will be done later in this report to ascertain if the model exhibits planar swimming.

4.1 Inertial force approximation

Figure 1 shows the simulated salamander model. This snap can be useful in understanding the concepts used for analysis, later in this report. It is necessary to have a knowledge of the coordinate frames which were used for the analysis of motion of the salamander model. Figure 2 shows the coordinate frames. x-y-z represent the frame in which we investigated the swimming motion of salamander model and x'-y' represent the body coordinate frame i.e. the frame in which forces were applied to the links. X-Y-Z represents

Figure 1: This picture presents a view of the simulated salamander model.

the global coordinate frame fixed to the enclosure in which the model was confined but it was not of much use in illustrating the motion of salamander model. The x-y-z frame represents a plane in which the model undergoes swimming motion at any instant and there is no movement of the model perpendicular to the plane at that time instant. To establish if the model exhibited planar swimming motion, the motion of salamander model was observed over a period of time and the position of center of mass of the model was recorded at some definite time instants. It was found out that the unit vectors between any two locations pointed almost in the same direction. This observation suggests that the motion of center of mass takes place along a particular direction. The approximate linear motion of the center of mass enabled us to assume a plane in which the motion of center of mass of the model took place. The average of unit vectors found above was taken as the longitudinal direction of motion of the model. The longitudinal component of velocity was calculated by taking dot product of the velocity of center of mass of the model in global coordinate frame, with the averaged unit vector which represented longitudinal direction of motion of the model.

To explain mathematically, if $\vec{v}$ is a vector in global coordinate frame with v_x,v_y,v_z as its components and $\vec{a}$ is the averaged unit vector, then longitudinal

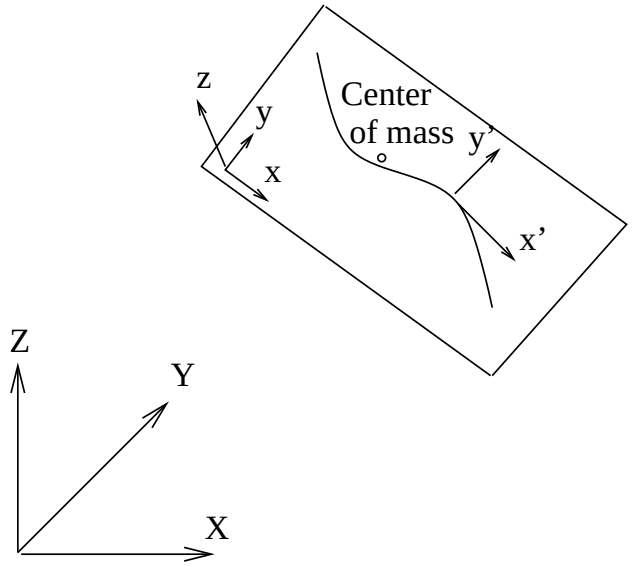

Figure 2: Depiction of coordinate frames encountered in the analysis of swimming motion of the salamander model. X-Y-Z is the global coordinate frame fixed to the domain in which the model undergoes swimming motion. x-y-z represents the coordinate frame which suggests the direction of motion of model at any instant. x'-y' signifies the body coordinate frame of the links i.e the frame attached to individual links and x' axis for a link represents the body axis of corresponding link at that instant.

component of velocity of the model is given by:

$$v_{long} = \vec{v} \cdot \vec{a} \tag{1}$$

and the magnitude of lateral component of velocity of the model is given by:

$$|v_{lat}| = \sqrt{v_x^2 + v_y^2 + v_z^2 - v_{long}^2} \tag{2}$$

This formulation was used extensively to calculate the longitudinal and lateral components of the position and velocity of the center of mass along with the components of forces acting on the model.

Now, we will have a look at the formulations used for the calculation of inertial forces acting on the links. The inertial model of force is attributed to the study by Ekeberg [1] of lamprey motion and the study by Ijspeert [2] of salamander motion who assumed that the speed of water relative to the salamander's body is very high for forces experienced by the creature to be mainly inertial (i.e. high Reynolds number). It was also assumed that the parallel and perpendicular components of forces can be calculated separately for each link (i=1,...,10) according to the formula:

$$F_{i,\parallel} = \lambda_{i,\parallel} v_{i,\parallel}^2 \tag{3}$$

$$F_{i,\perp} = \lambda_{i,\perp} v_{i,\perp}^2 \tag{4}$$

where

$$\lambda_{i,\parallel} = \frac{1}{2} C_{i,\parallel} S_i \rho \tag{5}$$

$$\lambda_{i,\perp} = \frac{1}{2} C_{i,\perp} S_i \rho \tag{6}$$

$v_{i,\parallel}$ and $v_{i,\perp}$ are the components of velocity of link i relative to water. $\lambda_{i,\parallel}$ and $\lambda_{i,\perp}$ are the coefficients that depend on density of the fluid ρ, the area perpendicular to movement S_i, and the drag coefficients $C_{i,\perp}$ and $C_{i,\parallel}$ that are dependent on the shape of link i. The links in our case were cuboidal in shape. Body x' direction (refer to Figure 2) represented parallel direction in the coefficients mentioned above and y' and z' directions were the perpendicular directions for which the drag coefficients were computed.

The values of drag coefficients in Table 1 were chosen for a particular case to get the representative plots of kinematics of the model and the dependence of swimming pattern of the model on drag coefficients will be demonstrated later in this report.

Before discussing the solution scheme for inertial model, it is very important to discuss the mechanism of swimming in biological salamander.

Travelling waves are produced in a salamander's body which propagate from its head to its tail. The changing shape of creature's body interacts with the surrounding water which exerts inertial and viscous forces on the body of salamander. These forces add up vectorially to provide propulsive force to the creature.

For the simulation of swimming motion in the model, we superimposed a sinusoidal travelling wave on the model by means of Proportional Derivative *(PD)* control functions. Equation of the travelling wave is given by Equation 7:

$$\theta_i^* = AMP * \sin[2\pi(f.t + (i\text{-}1).\phi)] \tag{7}$$

where

- θ_i^* is the desired angle at hinge i.
- AMP is the maximum possible value of θ_i^*.
- f is the frequency of travelling wave.
- t is the time instant at which θ_i^* is computed.
- ϕ is the phase difference between two successive hinges.

A PD controller produce the torque to be applied on a joint to follow a desired angle trajectory. The value of applied torque is calculated with the use of Equation 8.

$$T_i = \alpha(\theta_i^* - \theta_i) - \beta.\omega_i \tag{8}$$

where

- T_i is the applied torque at hinge i.
- α is the Proportional gain of PD controller.
- θ_i^* is the desired angle at hinge i.
- θ_i is the actual angle at hinge i.
- β is the Derivative gain of PD controller.
- ω_i is the rate of change of angle at hinge i.

The value of Proportional Gain was taken as 5.0 and the Derivative Gain was taken as 0.029. The frequency of travelling wave was taken as 0.8 Hz with its wavelength being equal to one body length of the model. The amplitude of travelling wave was taken as 0.4 radian i.e 22.91 ° which is a measure of

maximum angle at the hinge joint between two successive links. At this juncture, it will be very useful to have a look at the comparison of plots obtained for the angle desired between links at the hinge locations and the angle actually obtained by application of the PD Control functions with a set of parameters. There were 9 hinge joints between 10 links and for the purpose of analysis, we studied the angles obtained at first two hinges and at the middle hinge. Let θ_i be the actual angle at hinge i and θ_i^* be the desired angle at hinge i.

Figure 3(a), 3(b) and 3(c) give the comparison between θ and θ^* for hinges 1, 2 and 5 respectively. Figure 3(a) shows that the angle obtained at hinge 1 is same as the desired angle and the plot for θ_1 coincides with that of θ_1^*. Figure 3(b) shows that the values for θ_2 are same as that for θ_2^* except for a transient period in the beginning of motion of the model. It was important to study the behaviour of θ_5 as hinge 5 lies in the middle of body of the model and the highest torques are needed at the middle hinge. The results for θ_5 will therefore, represent the degree of coincidence of θ_i^* and θ_i for the entire model. As can be seen from Figure 3(c), there is a high degree of coincidence between the plot for θ_5 and the plot for θ_5^* except at the extreme values. But this degree of coincidence in the plots is the best possible considering the fact that we used same values of the Proportional and Derivatives gains for PD control of all the hinges.

Figure 4 represents variation in the torques applied to hinges 1, 2 and 5 respectively. It is clear from the plot that the applied torque had the maximum magnitude for hinge 5 which was quite apparent as we obtained the maximum degree of non-coincidence between the plots of θ and θ^* for hinge 5. Hence the torque required to bring the hinge angle to desired value was found to be maximum for hinge 5.

Now we proceed towards the description of solution scheme used for generating the motion of model when subjected to inertial forces in 2-D. The solution scheme consisted of the following sequence of operations:

1. Determination of components of velocity of the links in global coordinate frame i.e the X-Y-Z frame (refer to Figure 2).

2. Transformation of velocity obtained in step 1 to the coordinate frame linked to body of the links i.e the x'-y' frame (refer to Figure 2).

3. Calculation of inertial forces acting on the links (using Equations 3 and 4).

4. Applying inertial forces to respective links in their body coordinate frames using the functions provided by *ODE* software.

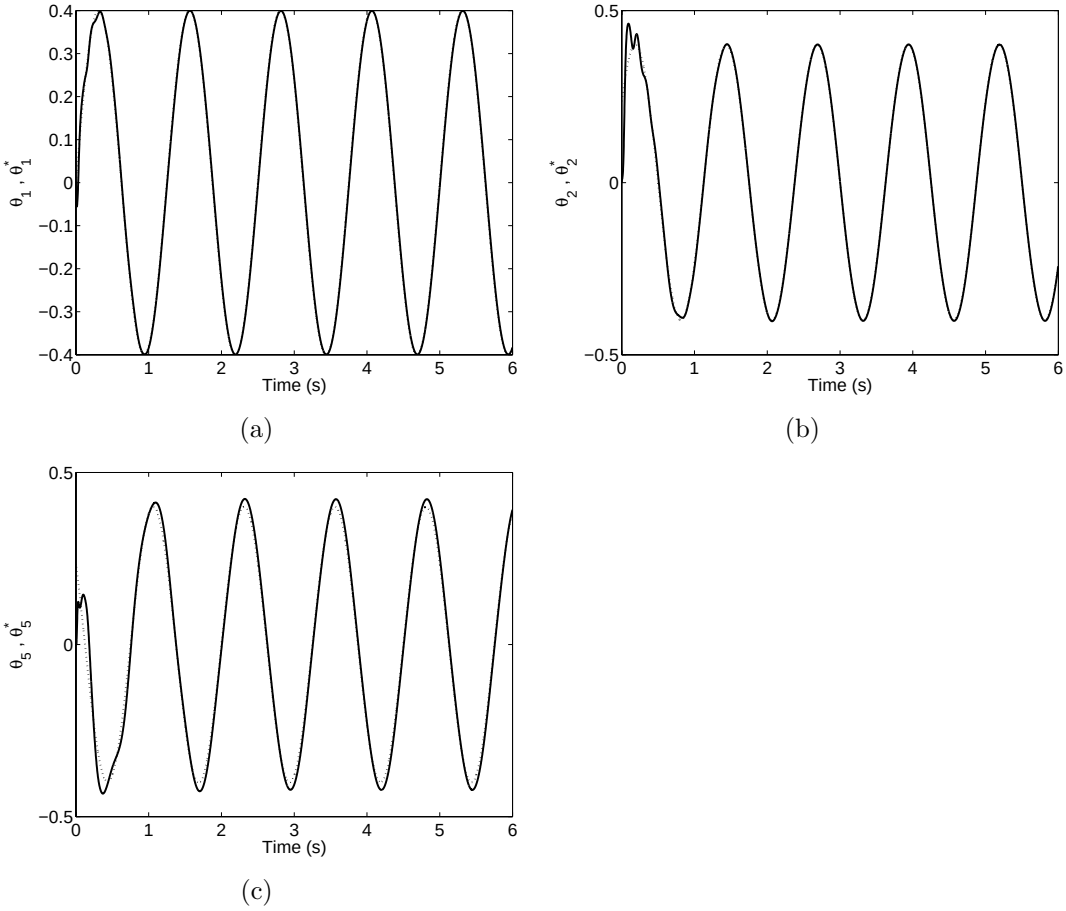

Figure 3: Plots for comparison between the desired angle at a hinge and the angle actually obtained between the links. Figures a, b and c present comparative plots for hinges 1, 2 and 5 respectively. The dotted curve denotes ${\theta_i}^*$ i.e the desired angle between the links at hinge i and the solid curve denotes θ_i i.e the angle actually obtained at hinge i.

Link i	$\lambda_{i,\parallel}$ (kg/m)	$\lambda_{i,\perp}$ (kg/m)
1	0.3	1.925
2	0.2	1.925
3	0.1	1.925
4	0.0	1.925
5	0.0	1.925
6	0.0	1.925
7	0.0	1.925
8	0.0	1.925
9	0.0	1.925
10	0.0	1.925

Table 1: Parameters for the mechanical simulation. Column 1 identifies the link for which drag coefficients are mentioned in subsequent columns. Column 2 gives the value of parallel drag coefficient whereas Column 3 mentions the perpendicular drag coefficient for corresponding link.

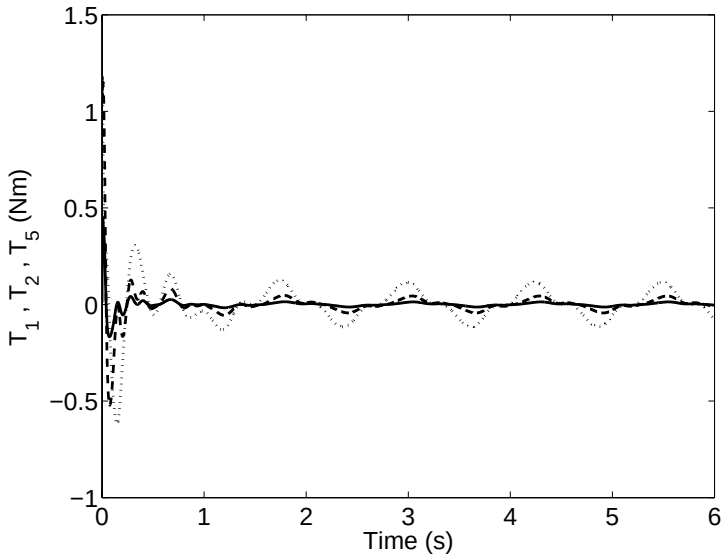

Figure 4: This figure gives the plot of applied torques at hinges 1, 2 and 5 respectively. The solid curve denotes the torque applied at hinge 1 i.e T_1. The dashed curve denotes T_2 and the dotted curve represents T_5.

5. Determination of velocity of the links and repetition of steps 2, 3 and 4.

ODE uses Euler integration technique for simulating a rigid body system through time. Each integration step advances the current time by a given step size, adjusting the state of all rigid bodies for the new time value.The specified step size in our case was 1 ms and the process was carried out for some time after which the velocity of model approached an asymptotic state at which the mean value of velocity components attained a steady value.

Figures 5(a) and 5(b) demonstrate the motion of center of mass of the salamander model in the frame of global coordinates where x-direction (refer to Figure 2) is the longitudinal direction of swimming. The x-coordinate of center of mass increases continuously and there is a fluctuation observed in the value of lateral displacement around zero. Inertial forces keep the salamander model on a straight line path with only a little deviation taking place in lateral direction. Figure 5(b) demonstrates fluctuations in the lateral position of center of mass of the model.

Figure 5(c) is the plot of longitudinal and lateral components of velocity of center of mass of the salamander model. The longitudinal component i.e. the x-component increases in the beginning when the travelling wave is initially superimposed on the model and goes on to attain a steady mean value of 0.24 m/s although there are small perturbations in its instantaneous value. There is a fluctuation observed in the magnitude of y-component and its mean value remains close to zero from the beginning of motion explaining why there was not an appreciable displacement in the lateral direction.

The linearity of longitudinal displacement motivates us to compare approximate slope of the plot of longitudinal displacement with the mean value of X-component of velocity. The approximate value of slope turns out to be 0.2384 m/s whereas the mean value of longitudinal component of velocity is 0.2394 m/s. This was expected observing a nearly linear pattern of motion of the simulated creature.

Figures 6(a) and 6(b) demonstrate the variation in forces on the center of mass in the lateral and longitudinal direction respectively. These forces were calculated using the following scheme:

1. Forces on the link i computed using Equations 3 and 4 were transformed to F_X and F_Y i.e the force components in global coordinate frame using the functions provided by *ODE* software.

2. Forces for links $i = 1 \cdots 10$ were added vectorially to obtain the force components on center of mass of the model in global coordinate frame i.e ${F_X}^{cm}$ and ${F_Y}^{cm}$.

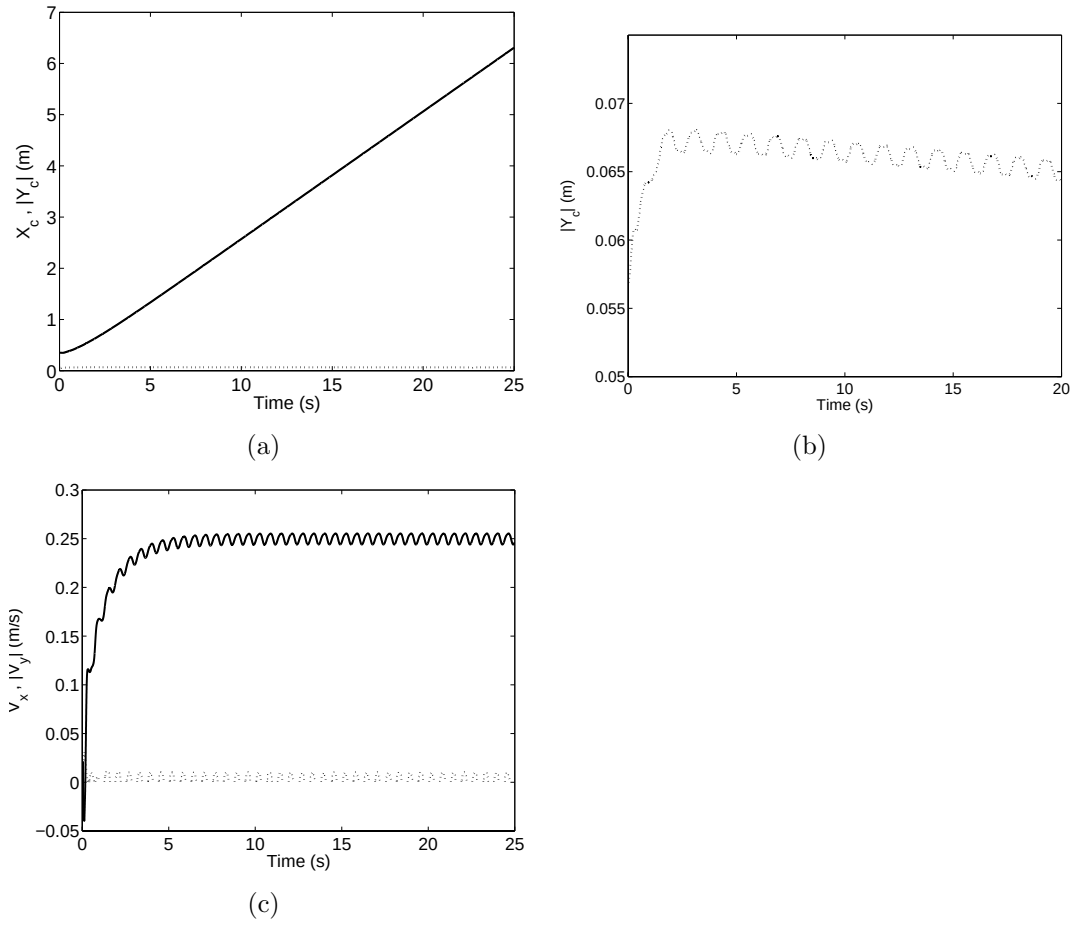

Figure 5: Kinematic description of the motion of salamander model subject only to inertial forces. Figure *a* represents the position of center of mass of the model. The solid curve gives the value of x-displacement or the longitudinal displacement and dotted curve provides the magnitude of y-displacement or the lateral displacement of center of mass. Figure *b* represents the magnitude of lateral displacement of the center of mass. This figure demonstrates the fluctuations in lateral position of the center of mass which is not very prominent against the longitudinal displacement of center of mass of the model. Figure *c* gives the velocity plot of center of mass of the model. The solid curve gives the value of V_x i.e the longitudinal component of velocity whereas the dotted curve provides the absolute value of lateral component of velocity, V_y.

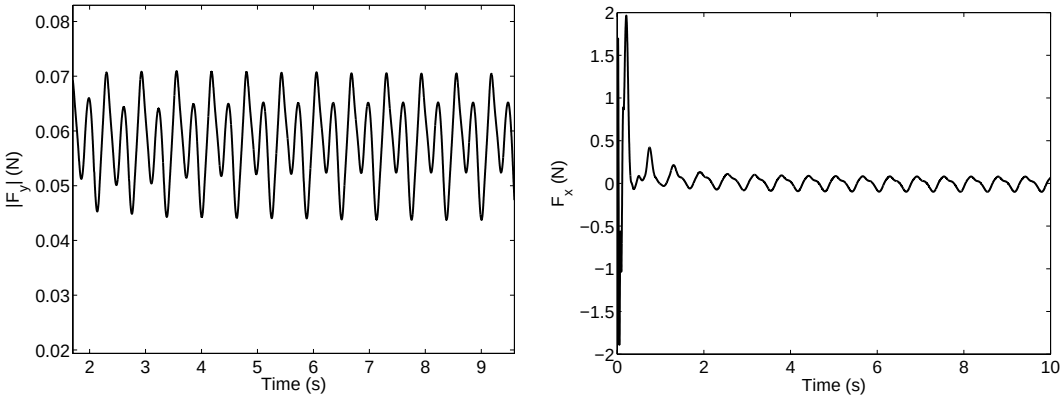

(a) (b)

Figure 6: Figure *a* demonstrates fluctuations in the magnitude of lateral force on center of mass of the model i.e the force on the model in y-direction. Figure *b* represents the variation in longitudinal component of the force acting on center of mass of the model.

3. F_{long} and F_{lat} i.e the longitudinal and lateral components of force were obtained by subjecting ${F_X}^{cm}$ and ${F_Y}^{cm}$ to the techniques described in Equations 1 and 2.

Fluctuation in the forces can be attributed to the travelling wave superimposed on the salamander model.

4.2 Demonstration of swimming motion of the model.

Figure 7 demonstrates the swimming motion of salamander model under the influence of inertial forces. The travelling wave is superimposed on the model and inertial forces acting on the model due to subsequent motion of the model provide propulsive force to the model which takes it ahead. The travelling wave can be identified from Figure 7 by observing curvature in the body of salamander model. It is evident from Figure that the model advances in longitudinal direction with hardly any displacement in lateral direction.

After this analysis, we proceeded towards an approach in which we considered both inertial as well as viscous forces.

4.3 Incorporation of viscous forces in the analysis

The Reynolds number for a flow characterises the ratio of inertial forces acting on the flow to viscous forces developed in the flow. High Reynolds

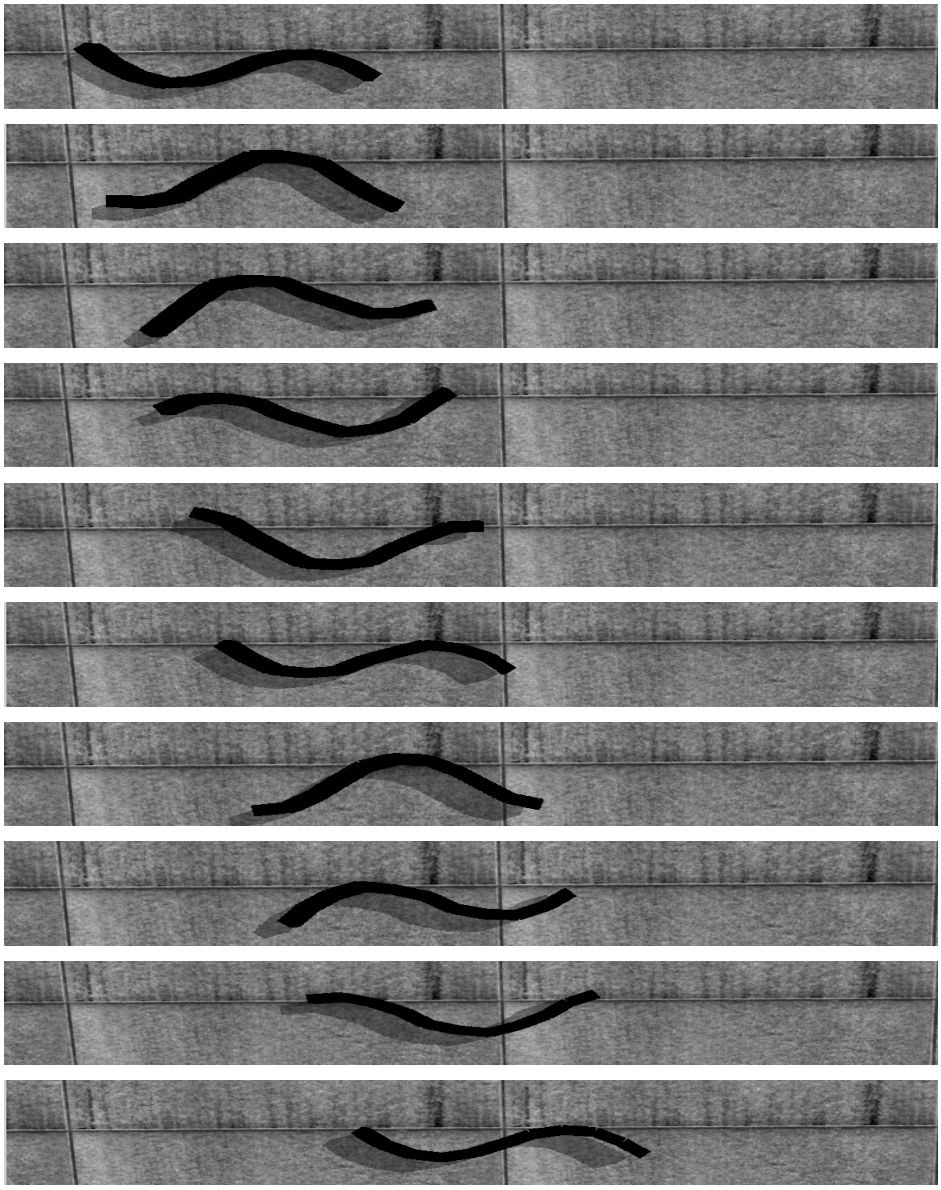

Figure 7: Mechanical simulation of swimming of the salamander model. Successive snaps of the motion of salamander model demonstrate longitudinal advance of the model with a little lateral deflection. The curvature in the body of salamander model signifies the travelling wave superimposed on the model.

number flow signifies greater inertial forces in comparison to viscous forces. Formally, the Reynolds number can be expressed as:

$$Re_L = \rho * V * L/\mu \tag{9}$$

where L is the characteristic length of flow phenomena which in this case is the length of body and V is the characteristic velocity of flow. μ is the dynamic viscosity of fluid (Nsm^{-2}). The Reynolds number for swimming movement of salamander model in inertial case corresponding to the maximum value of longitudinal component of velocity and length of the model, taken as the characteristic length, came out be 1.88×10^5 which was fairly high. For flow over a flat plate, Reynolds number of 10^5 signifies higher inertial forces as compared to viscous forces. Although the problem is not similar to a flat plate problem, the value of Reynolds number calculated for inertial problem probably indicates higher inertial forces as compared to viscous forces. The analysis done in coming sections might help us to predict the relative magnitudes of inertial and viscous forces. The calculation of viscous forces (i.e. shear forces) on the links was done using three different schemes. One schemes involved the calculation of forces from a linear model in which the shear stress is proportional to velocity of the link. The other two schemes were developed using the formulations for laminar boundary layer flow over a flat plate. Main motivation for the use of three schemes was to obtain the variation of viscous forces with the degree of velocity used in the formulations for viscous forces, as will be discussed in the following sections.

4.3.1 Linear model of viscous forces

The magnitude of shear stress at a point on the surface of an object moving through a fluid depends upon the value of velocity gradient at that point in the normal direction. If x is the direction of movement of the object, then the shear stress is found from Muralidhar [3] as:

$$\tau = \mu(du/dy) \tag{10}$$

where τ is the shear stress, μ is the coefficient of dynamic viscosity and du/dy is the velocity gradient in normal direction. For the linear approximation, the gradient can be approximated as V/δ where V is the velocity of center of mass of the link and δ is the boundary layer thickness. δ can be approximated as $L/\sqrt{Re_L}$ where L is the length of body and the same can be put into Equation 10. The viscous force acting on each surface of the link will then be given by:

$$F_v = \tau A \approx \mu(V/\delta)A \approx \mu VA(\sqrt{Re_L}/L) \tag{11}$$

where F_v is the viscous force and A is the area of surface on which the viscous force is acting. The Reynolds number value used in Equation 11 was the one mentioned in previous section of this report.

Figure 8(a) gives a comparison between the inertial and viscous components of the longitudinal force acting on center of mass of the salamander model. Similarly, Figure 8(b) provides a comparison between the magnitude of inertial and viscous components of the lateral force acting on center of mass of the salamander model. These force components were computed using the scheme mentioned for computing the components of inertial force in Section 4.1. The striking aspect of above plots is the dominance of inertial forces over viscous forces.

Figure 8(c) presents the fluctuations in velocity components of the salamander model with time. The mean longitudinal component came out to be 0.1997 m/s. Here, the mean value is less as compared to the purely inertial case due to viscous forces coming into play but viscous forces do not bring about a very large change in the velocity plot as compared to the one obtained for purely inertial scheme. This fact will be highlighted by the study of swimming motion of the model when subjected to viscous forces according to the other two schemes.

4.3.2 Quadratic scheme of viscous forces

This model was worked out making the assumption that the fluid flow over the links lies in the laminar regime. Treating the flow over the links as a laminar boundary layer flow over a flat plate, we used the formulations for shear forces in a flat plate boundary layer problem. The average drag coefficient for flow over an object is defined as:

$$C_D = \tau/(\frac{1}{2}\rho V^2) \tag{12}$$

where

- τ is the shear stress exerted by the fluid at solid surface.
- ρ is the density of fluid.
- V is the relative velocity between the two medium.

For a flat plate problem, the average drag coefficient over the length of plate is found out from Muralidhar [3] as:

$$C_D = 1.328/\sqrt{Re_L} \tag{13}$$

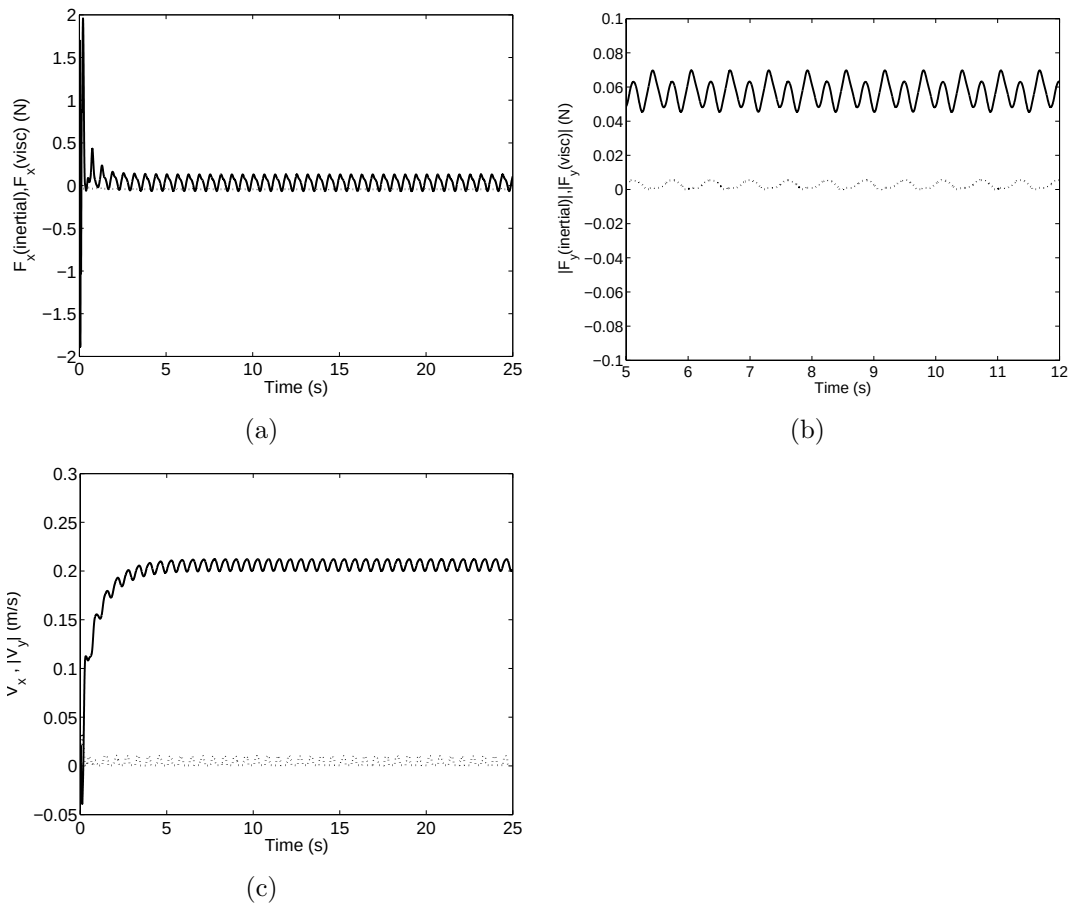

Figure 8: Plots for linear scheme: Figure a demonstrates the contribution of inertial and viscous forces to the longitudinal force acting on center of mass of the model. The solid curve represents inertial contribution to the longitudinal force whereas dotted curve represents the contribution of viscous forces to the force on center of mass in the longitudinal direction. Figure b gives the contribution of inertial and viscous forces to the lateral force acting on center of mass of the model. The solid curve represents the magnitude of inertial contribution to the lateral force whereas dotted curve represents the contribution of viscous forces to the force in z-direction. Figure c gives velocity plot of the model with solid line representing V_x i.e the longitudinal component of velocity and dotted line representing abs(V_y) i.e the magnitude of lateral component of velocity of center of mass of the model.

In this case, Re_L was calculated using the maximum velocity of inertial case and V took the value of components of velocity of center of mass of the link for the computation of viscous forces in x' and y' directions of the body coordinate frame. Viscous force acting on each surface of the link is given by:

$$F_v = C_D(\frac{1}{2}\rho V^2)A = 1.328(\frac{1}{2}\rho V^2)A/\sqrt{Re_L} \tag{14}$$

where A is area of the surface for which viscous force is calculated.

Figures 9(a) and 9(b) demonstrate fluctuations in the value of inertial and viscous components of the longitudinal and lateral forces respectively, acting on center of mass of the salamander model. These plots also show that inertial forces are much higher in magnitude than viscous forces and so the movement of salamander model in this case, was primarily influenced by inertial forces.

Figure 9(c) gives fluctuations in the velocity components of center of mass of the model. The mean longitudinal velocity in this case turned out to be 0.1776 m/s which was less as compared to mean longitudinal velocity for the linear model of viscous forces.

4.3.3 Extension of quadratic scheme of viscous forces

This model was an extension of previous model in the sense that in this model, we used same formulations as presented in the previous section for calculating viscous forces. Using the formulations for C_D as mentioned in Equations 12 and 13 and the formulation for F_v (Equation 14), the expression for viscous force on a surface turned out to be:

$$F_v = C_D(\frac{1}{2}\rho V^2)A = 1.328(\frac{1}{2}\rho V^2)A/\sqrt{Re_l} \tag{15}$$

where

$$Re_l = \rho * V * l/\mu \tag{16}$$

This method was different from previous analysis in the sense that we put the formulation for Reynolds number (Equation 16) in Equation 15 rather than using a constant value for Reynolds number, as we have been doing in previous two schemes of viscous forces. V in this case was the instantaneous velocity component of center of mass of the link and l was the significant dimension of link for computing the shear stress which was length or breadth of the link depending upon the surface for which shear stresses were computed. Therefore,

$$F_v = 0.664\rho V^{3/2}A/\sqrt{\rho l/\mu} \tag{17}$$

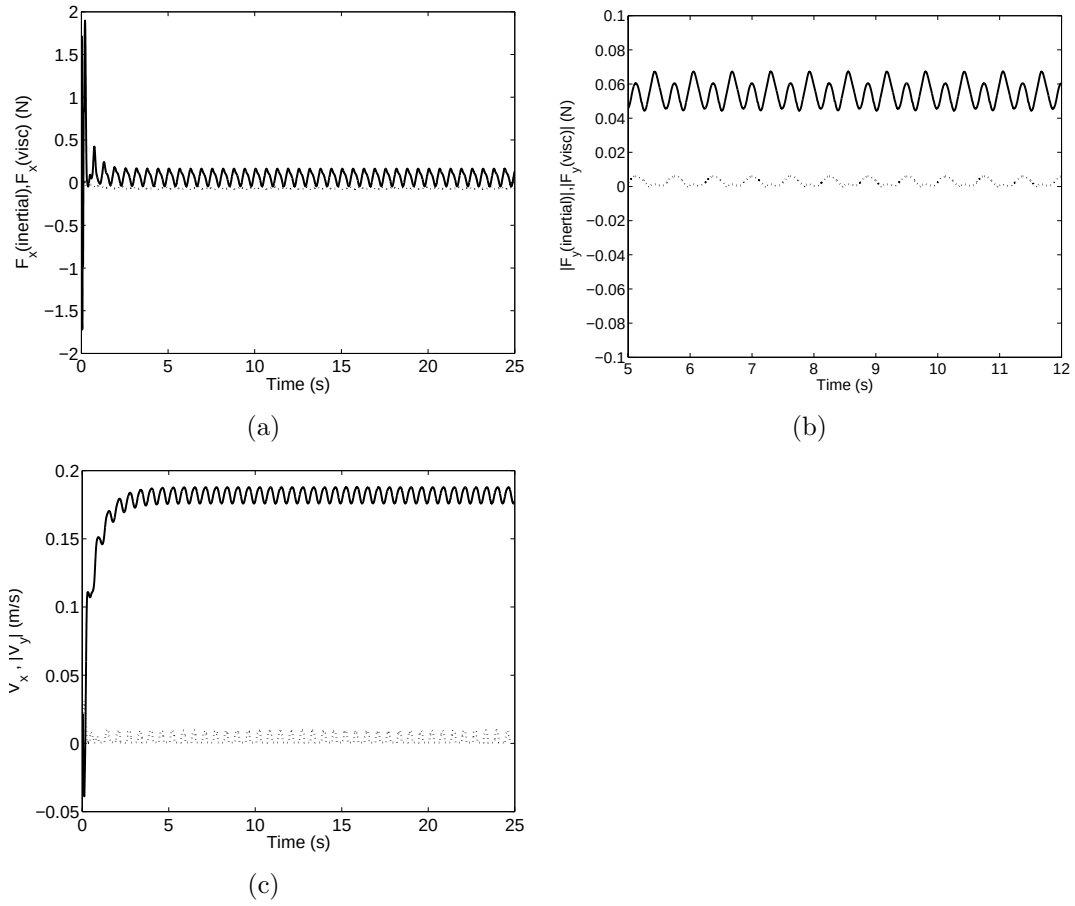

Figure 9: Plots for quadratic scheme: Figure a demonstrates the contribution of inertial and viscous forces to the longitudinal force acting on center of mass of the model. The solid curve represents inertial contribution to the longitudinal force whereas dotted curve represents the contribution of viscous forces to force on the center of mass in x-direction. Figure b gives the contribution of inertial and viscous forces to the lateral force acting on center of mass of the model. The solid curve represents the magnitude of inertial contribution to the lateral force whereas dotted curve represents the contribution of viscous forces to the force in y-direction. Figure c gives velocity plot of the model with solid curve representing V_x i.e the longitudinal component of velocity and dotted line representing abs(V_y) i.e the absolute value of lateral component of velocity of center of mass of the model.

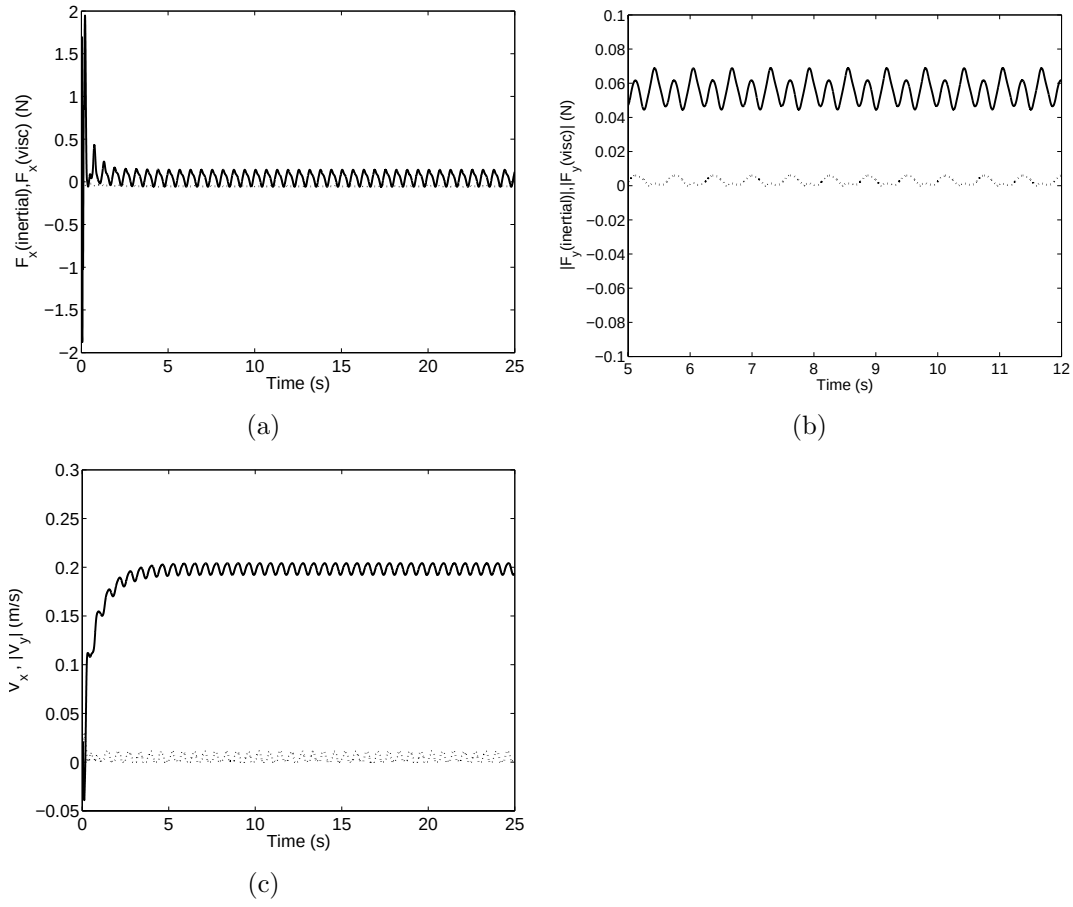

Figure 10: Plots for power *3/2* scheme: Figure *a* demonstrates the contribution of inertial and viscous forces to the longitudinal force acting on center of mass of the model. The solid curve represents inertial contribution to the longitudinal force whereas dotted curve represents the contribution of viscous forces to the force on center of mass in the x-direction. Figure *b* gives the contribution of inertial and viscous forces to the lateral force acting on center of mass of the model. The solid curve represents the magnitude of inertial contribution to the lateral force whereas dotted curve represents the contribution of viscous forces to the force in y-direction. Figure *c* gives velocity plot of the model with solid curve representing V_x i.e the longitudinal component of velocity and dotted curve representing abs(V_y) i.e the absolute value of lateral component of velocity of center of mass of the model.

Figures 10(a) and 10(b) present variations in inertial and viscous components of the lateral and longitudinal forces experienced by center of mass of the salamander model. In this case too, we find the magnitude of inertial forces being much higher than that of viscous forces.

Figure 10(c) exhibits fluctuations in the components of velocity of center of mass of the salamander model. The mean value of x-component came out to be 0.1926 m/s which lies between the values, we found for mean longitudinal component of velocity for the purely inertial scheme and linear viscous scheme on one side and the quadratic viscous scheme on other side.

4.4 Comparison of schemes suggested for the computation of inertial and viscous forces

In this section, we will try to bring about a comparison between the behaviour of salamander model when subjected to different schemes of force computation, we have discussed so far. This is essential from the point of view of assessing the relative importance of inertial and viscous forces.

Figure 11 gives a comparative plot of the longitudinal component of velocity of the salamander model with respect to time for four schemes discussed so far.

The plot at the top corresponds to purely inertial scheme whereas the plots below are the one which envisage both inertial as well as viscous forces. The relative nature of plots came out as predicted since introduction of viscous forces to the model was certain to bring about a reduction in the magnitude of velocity of progression of the model. It was interesting to analyse the relative nature of plots for the schemes envisaging viscous forces. From the plot, it is evident that among the schemes involving the viscous forces, the mean longitudinal component of velocity was greatest for the linear scheme and least for the quadratic scheme of viscous forces. This was expected as for high speed flows, v^2 term dominates the term which is linear in v and so the quadratic scheme involving viscous forces proportional to v^2 damped motion of the model to a greater extent as compared to the linear model of viscous forces, which involved the application of viscous forces proportional to v. Experimentation with the salamander robot will determine real velocity plot for the model and will also help to ascertain the relative influence of various inertial and viscous forces on the swimming model.

Out of the three schemes suggested for viscous forces, we consider the linear viscous scheme as the most realistic as it was obtained from the basic laws governing boundary layer formation over an object moving through a fluid. The other two schemes were obtained by bringing about some modifications

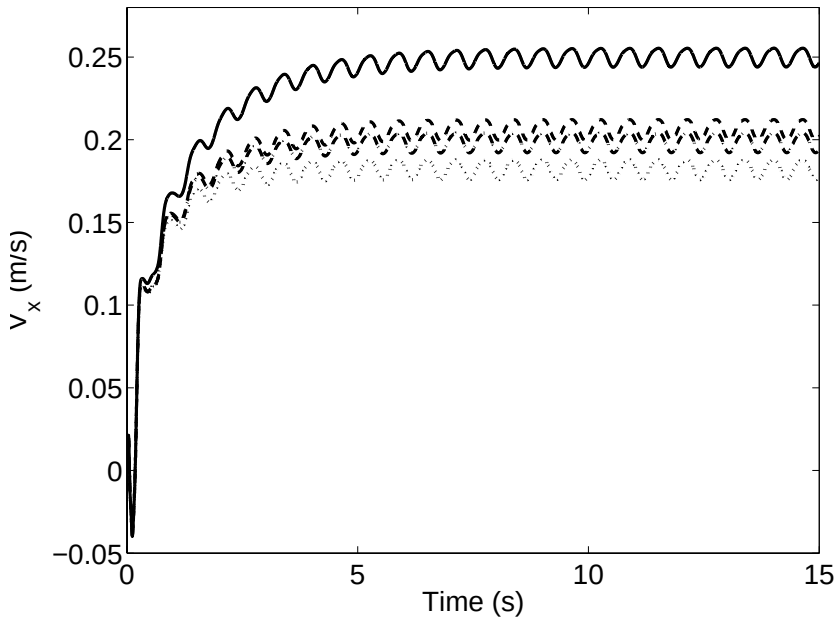

Figure 11: This figure gives plots of the longitudinal component of velocity for four schemes. V_x represents the longitudinal component of velocity of center of mass of the model. The solid curve gives V_x plot for purely inertial case. The dashed curve lies immediately below the inertial curve and it represents the linear scheme for viscous force computation. The dash-dot curve representing power *3/2* viscous model, lies below the plot of linear viscous model and the dotted curve representing the quadratic model of viscous force computation, lies below the other three plots.

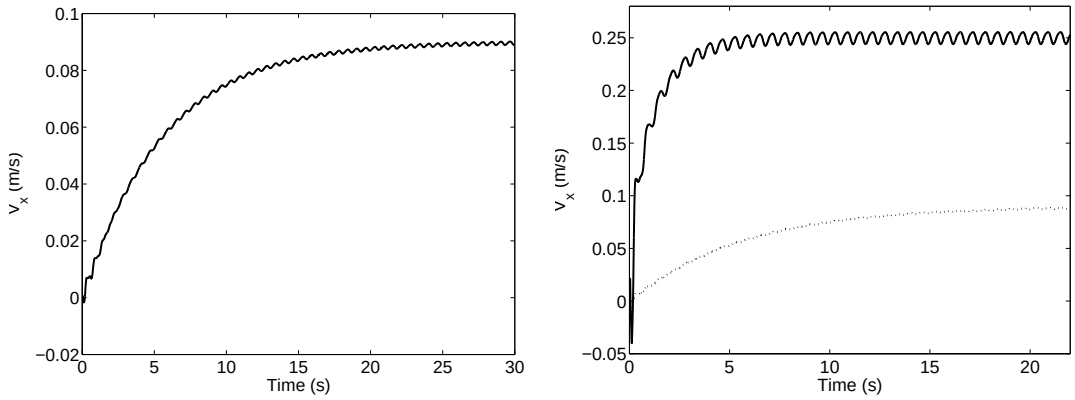

(a) (b)

Figure 12: Figure a presents velocity plot for the model subject to purely viscous forces: This figure represents the case in which only viscous forces were applied on the model from the beginning of its motion. V_x is the longitudinal component of velocity of the model. Figure b compares the longitudinal speed attained by the model for purely viscous case with the longitudinal speed attained in purely inertial case, discussed in Section 4.1. The solid curve represents V_x for inertial case whereas dotted curve denotes V_x for viscous case.

in the formulations for viscous drag for laminar boundary layer flow over a flat plate which was a very strong assumption for relative motion between the model and surrounding fluid. The main motive behind the inclusion of viscous forces of higher degree of v was to show that for high speed flows, drag acting on the flow increases with increase in the degree of v present in the formulation for viscous forces.

4.5 Analysis of swimming motion of the model in a purely viscous medium

This analysis was done with the aim of gaining insight into the motion of salamander model when it encounters a medium where it is subjected to purely viscous forces.

Figure 12(a) represents the case in which the model was subjected only to viscous forces from the beginning of its motion. The mean longitudinal velocity came out to be 0.0733 m/s. Figure 12(b) presents the comparison which can be done between the velocity plot for purely viscous case and the plot obtained for V_x, for purely inertial case. Figure 12(b) shows that the transient time interval after which the salamander model attains a stable value of V_x when subjected to only viscous forces was about 17 seconds

whereas the time taken in the scheme involving only inertial forces was about 5 seconds. This large difference in the time intervals gives an indication of the probable dominance of inertial forces over viscous forces for the swimming motion of salamander model driven by travelling waves of high frequency.

4.6 Sensitivity of swimming motion of the model to parallel drag coefficient $\lambda_{i,\parallel}$

In this section, dependence of the velocity of salamander model on the parallel drag coefficient i.e. $\lambda_{i,\parallel}$ will be demonstrated. The scheme for analysis centers around drag coefficient for the first link as it is the first link which directly faces the fluid. The remaining links are exposed to the fluid later so that they do not experience the same resistance as experienced by first link. The value of drag coefficients are determined experimentally for different geometries and we did not have the data for parallel drag coefficient of different links. We worked upon five different schemes, each one of them sugggesting a certain variation in the value of drag coefficients for different links. For this analysis, the value of $\lambda_{1,\parallel}$ was varied from 0.1 to 0.9 in steps of 0.05. The five schemes mentioned above can be understood by defining a ratio r_i where

$$r_i = \lambda_{i,\parallel}/\lambda_{1,\parallel} \tag{18}$$

Table 2 shows the five schemes used for representing variation in the value of parallel drag coefficient of the links relative to $\lambda_{1,\parallel}$.

The drag coefficients were set to the values mentioned in Table 2 and the variation in longitudinal component of velocity was obtained. The mean values of longitudinal component of velocity were plotted against the corresponding value of $\lambda_{1,\parallel}$.

Figure 13(a) shows the five schemes suggested for obtaining variation in the value of parallel drag coefficient of the links. The value of r_i for a particular scheme for a particular link signifies the parallel drag coefficient of that link with respect to $\lambda_{1,\parallel}$. Figure 13(b) shows the variation of mean value of the longitudinal component of velocity with respect to $\lambda_{1,\parallel}$ for all five schemes. $\lambda_{1,\parallel}$ was chosen as the parameter for analysis.

All plots in Figure 13(b) suggest that the mean value of longitudinal component of velocity of the model decreases as we proceed towards the higher values of drag coefficients which is obvious as high values of drag coefficients signify greater opposition to the motion of salamander model. As compared to the other four schemes, the third scheme showed a relatively higher values of the mean x-component of velocity for same values of $\lambda_{1,\parallel}$. This happened because drag coefficients of the links 2 to 10 experienced a sharper decrease

Link i	$(r_{i,1})$	$(r_{i,2})$	$(r_{i,3})$	$(r_{i,4})$	$(r_{i,5})$
1	1.000	1.0000	1.000	1.0	1.0
2	0.667	0.5000	0.333	0.9	1.0
3	0.333	0.2500	0.111	0.8	1.0
4	0.167	0.1250	0.037	0.7	1.0
5	0.083	0.0625	0.020	0.6	1.0
6	0.083	0.0625	0.020	0.5	1.0
7	0.083	0.0625	0.020	0.4	1.0
8	0.083	0.0625	0.020	0.3	1.0
9	0.083	0.0625	0.020	0.2	1.0
10	0.083	0.0625	0.020	0.1	1.0

Table 2: This table provides the information about five different schemes considered for analysis of sensitivity of the model to parallel drag coefficient of the links. $r_{i,j}$ is the ratio of parallel drag coefficient of link i with respect to $\lambda_{1,\|}$, for the Scheme j. Column 1 identifies the link for which value of r_i will be mentioned in the same row. The other five columns depict variations in the value of parallel drag coefficients present in five different schemes.

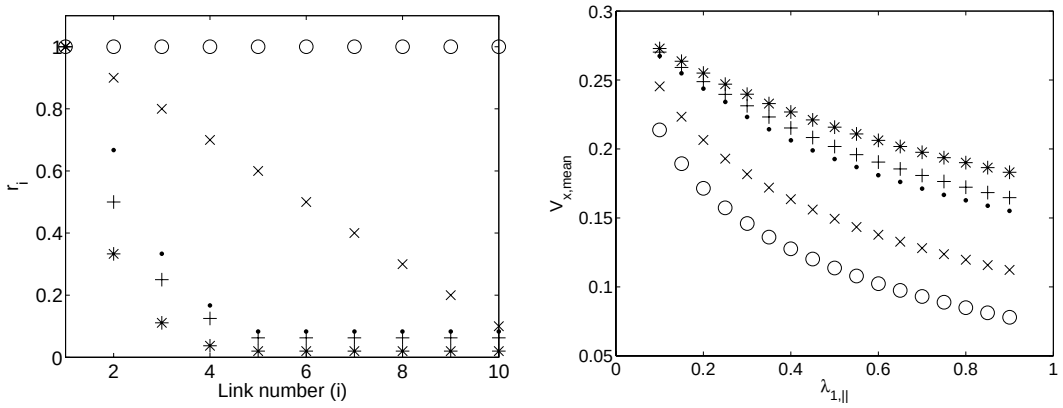

(a) (b)

Figure 13: Figure a graphically represents five different schemes. The link number i is mentioned as x-coordinate of the plot and r_i is plotted on the y-axis. The five different schemes are shown by $\cdot$, + , * , x and o respectively. Figure b demonstrates variations in $V_{x,mean}$, the mean value of longitudinal component of velocity with respect to $\lambda_{1,\|}$ which was chosen as the reference for sensitivity analysis. The results of five different schemes have been shown by $\cdot$, + , * , x and o respectively, for the corresponding scheme in Figure a.

in value with respect to $\lambda_{1,\parallel}$ in the third scheme as compared to that in the other four schemes. Thus relatively lower values of drag coefficients for links 2 to 10 for same value of $\lambda_{1,\parallel}$ amounted to a lower overall drag and hence higher values of the mean longitudinal component of velocity.

5 Analysis of slow swimming motion of the salamander model

In this section, slow swimming motion of the salamander model will be discussed. Slow swimming denotes low Reynolds number associated with the relative motion between the model and surrounding fluid. This analysis is, therefore more of a qualitative analysis in which we will compare the influence of inertial and viscous forces over the motion of model at slow swimming speeds. At low swimming speeds, inertial forces acting on the moving model are not very important and so it was very difficult to correctly ascertain the drag coefficients necessary for computing inertial forces as described in Section 4.1. Moreover, we intended to use the linear scheme of viscous forces as the formulations determining viscous forces as defined in Section 4.3.1. The formulation of viscous forces was given in Section 4.3.1 as:

$$F_v = \tau A \approx \mu(V/\delta)A \tag{19}$$

This equation can be written as:

$$F_v \approx k(V)A \tag{20}$$

where k is a constant whose value was approximated using the value of dynamic viscosity (μ) of water and the typical value of boundary layer thickness δ for a slow speed problem. For slow speed of relative motion between an object and a fluid, the boundary layer thickness δ is very small. Hence for the linear case, we took the boundary layer thickness to be of the order of 0.01 mm to get the value of k to calculate viscous forces.

As the swimming speed of salamander model depends largely upon the frequency of travelling wave superimposed on the model, the frequency of travelling wave was brought down from 0.8 Hz to 0.2 Hz.

The slow speed problem was addressed by considering three cases:

1. Model subjected to only inertial forces.
2. Model subjected to inertial as well as viscous forces.
3. Model subjected to only viscous forces.

The value of drag coefficients for calculating inertial forces were kept the same as that in Section 4.1 and are mentioned in Table 3. At low Reynolds number, inertial terms in the Navier-Stokes equation are relatively unimportant; the flow pattern is determined by viscous forces. As a consequence, the expressions for velocity, drag forces, and the like do not involve the fluid density directly. However, the value of drag coefficients were kept the same as in previous cases as we did not have explicit formulations for calculating the drag coefficients at low swimming speeds.

Link i	$\lambda_{i,\parallel}$ (kg/m)	$\lambda_{i,\perp}$ (kg/m)
1	0.3	1.925
2	0.2	1.925
3	0.1	1.925
4	0.0	1.925
5	0.0	1.925
6	0.0	1.925
7	0.0	1.925
8	0.0	1.925
9	0.0	1.925
10	0.0	1.925

Table 3: Parameters for mechanical simulation in the slow swimming problem. Column 1 identifies the link for which drag coefficients are mentioned in subsequent columns. Column 2 gives the value of parallel drag coefficient whereas Column 3 mentions the perpendicular drag coefficient for corresponding link.

5.1 Analysis involving only inertial forces.

Figure 14 represents the motion of model under slow swimming conditions and subjected only to inertial forces calculated using Equations 3 and 4 described in Section 4.1 and the values of drag coefficients mentioned earlier in this section. The longitudinal component of velocity i.e V_x attained a mean value of 0.0542 m/s. This plot alone does not convey much information about the extent of influence of inertial forces on the swimming of salamandet model at low swimming speeds. So we proceed to next section in which the model will be subjected to both inertial as well as viscous forces.

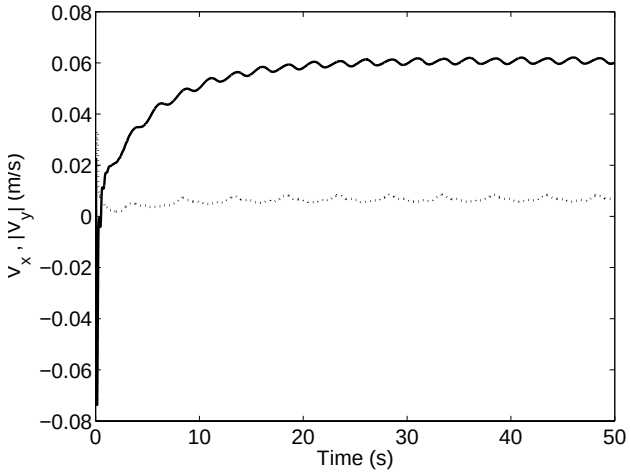

Figure 14: This figure gives the velocity plot of the slow swimming motion of salamander model subject only to inertial forces with the solid curve representing V_x i.e the longitudinal component of velocity and dotted curve representing abs(V_y) i.e the magnitude of lateral component of velocity of center of mass of the model.

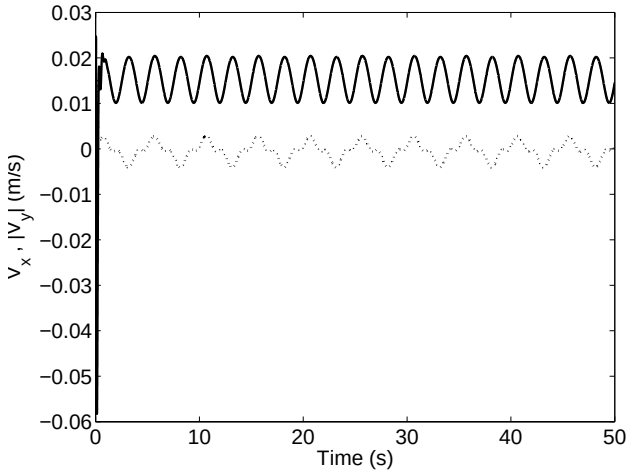

Figure 15: This figure gives the velocity plot of slow swimming motion of the model subject to inertial as well as viscous forces with the solid curve representing V_x i.e the longitudinal component of velocity and dotted curve representing V_y i.e the lateral component of velocity.

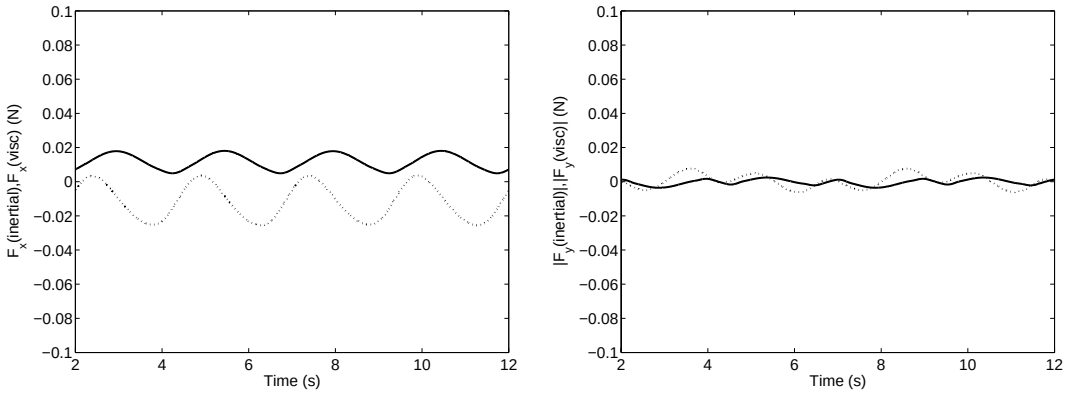

(a) (b)

Figure 16: Plots for slow speed swimming of the model subject to both inertial as well as viscous forces: Figure *a* demonstrates the contribution of inertial and viscous forces to the longitudinal force acting on center of mass of the model. The solid curve represents inertial contribution to the longitudinal force whereas dotted curve represents the contribution of viscous forces to the force on center of mass, in the longitudinal direction. Figure *b* gives the contribution of inertial and viscous forces to the lateral force acting on center of mass of the model. The solid curve represents inertial contribution to the lateral force whereas dotted curve represents the contribution of viscous forces to the force in lateral direction.

5.2 Application of inertial as well as viscous forces to the model.

In this case, the model was subjected simultaneously to inertial and viscous forces. The viscous forces were calculated using the formulations described earlier in this section. Figure 15 shows variation in the components of velocity of center of mass of the model. The longitudinal component of velocity, V_x had a mean value of 0.0152 m/s and this value was lower compared to values obtained in Section 5.1. The lateral component of velocity, V_y fluctuates around zero and the mean value of V_y stays very close to zero.

Figures 16(a) and 16(b) give the contribution of inertial and viscous forces to the forces acting on center of mass of the model. Both the plots demonstrate that viscous forces make a greater contribution to the longitudinal and lateral forces acting on center of mass of the model. In next section, we will study the motion of model subject only to viscous forces.

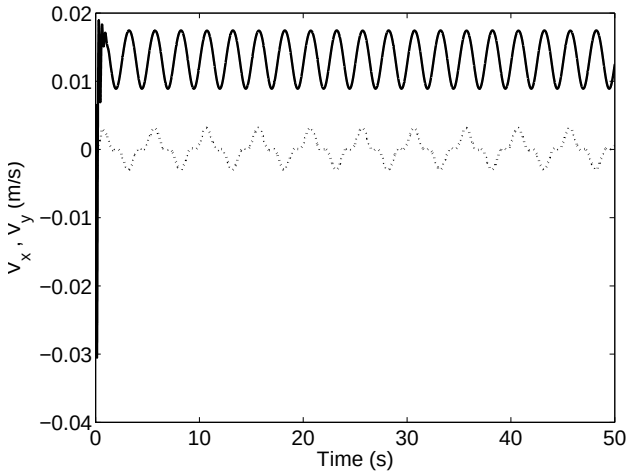

Figure 17: This figure gives the velocity plot of slow swimming motion of the model subject only to viscous forces with the solid curve representing V_x i.e the longitudinal component of velocity and dotted curve representing V_y i.e the lateral component of velocity of center of mass of the model.

5.3 Analysis of swimming motion of the model subject only to viscous forces.

This section aims at studying the motion of salamander model subject only to viscous forces. Figure 17 shows the velocity plot for motion of the model when only viscous forces were applied to it. The longitudinal velocity, V_x had a mean value of 0.0132 m/s which is lowest of all the three cases discussed so far. The lateral component of velocity, as in the earlier cases had a mean value very close to zero. In next section, we cmparatively analyse the results obtained for three cases discussed for the slow speed problem.

5.4 Comparison of force schemes used for analysing slow swimming motion of the salamander model.

This section aims at the comparative analysis of three force schemes discussed earlier in this section and used for the analysis of slow swimming motion of the salamander model. Figure 18 demonstrates variations in the longitudinal component of velocity for three force schemes discussed in Sections 5.1, 5.2 and 5.3 respectively. Figure 18 shows that inertial forces might not be very prominent in determining the slow swimming motion as the plot corresponding to purely inertial case attains a higher value of the velocity as compared

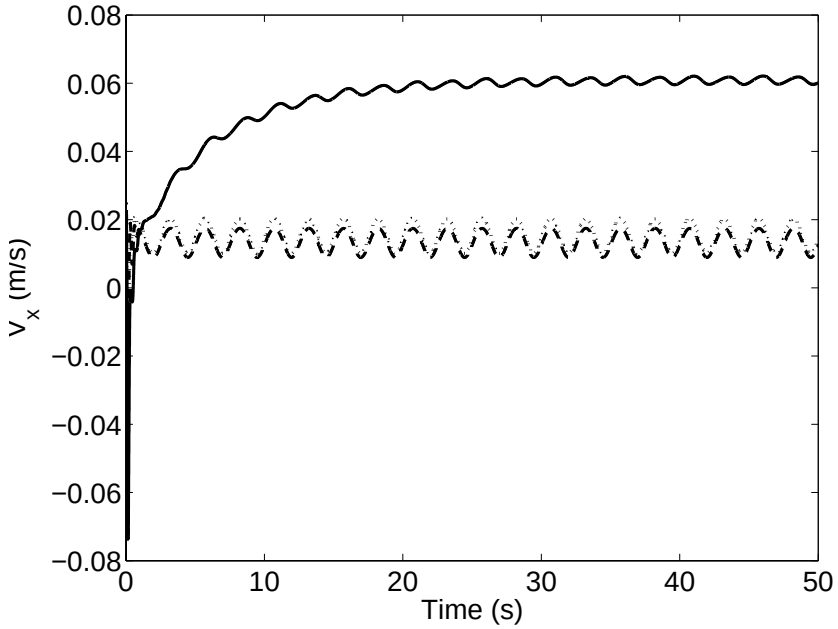

Figure 18: This figure gives the plot of longitudinal component of velocity for three force schemes. V_x represents the longitudinal component of velocity of center of mass of the model. The solid curve gives V_x plot for purely inertial case. The dotted curve lies below the inertial curve and it represents the scheme in which the model was subjected to inertial as well as viscous forces. The dashed curve represents the results for purely viscous scheme and it lies below the plots for other two schemes.

to the other two schemes. Plots for the other two schemes discussed in Sections 5.2 and 5.3 almost coincide, indicating the dominant role which viscous forces might play over inertial forces, in determining slow swimming motion of the salamander model.

As mentioned earlier, this study does not accurately reflect the prominence of one type of force over another force. Intuitively, at slow swimming speeds, viscous forces must dominate the motion of model. This study can be considered as a qualitative analysis of various forces at low swimming speeds. Experiments performed on a salamander robot will help to analyse the quantitative influence of inertial and viscous forces and those results can also be compared with the results of this analysis to ascertain the accuracy of this analysis, both qualitatively and quantitatively.

6 Analysis of salamander model under the influence of forces in 3-D

In Section 4, we studied the motion of salamander model subject to inertial and viscous forces in 2-D. This section extends that analysis by incorporating forces in the 3^{rd} dimension and then studying the motion of model under the influence of forces in 3-D. With the motive to study 3-D motion of the model, we applied initial external forces and torques to the model to give initial translational and rotational accelerations respectively to the plane in which the model swims and analysed the motion of plane with respect to time. We used two schemes to impart initial accelerations (translational and rotational) to the plane which were as follows:

1. Translational Perturbations: All the body links were subjected to an initial force of -0.1 N in the -ve Z (refer to Figure 2) direction at the beginning of motion for a time span of 5 seconds and the applied forces were removed after the mentioned time span. The subsequent motion of model was studied to analyse the influence of initial forces.

2. Rotational Perturbations: All the body links were subjected to an initial torque of 0.001 Nm about the x' axis which was the body coordinate axis of a link as explained in Figure 2, for a time span of 5 seconds and the applied moments were then removed. The effect of initial torques on the model was then analysed.

Figures 19(a) and 19(b) respectively depict the application of initial translational and rotational perturbations to the salamander model. Having worked out the nature of initial forces and torques required to render

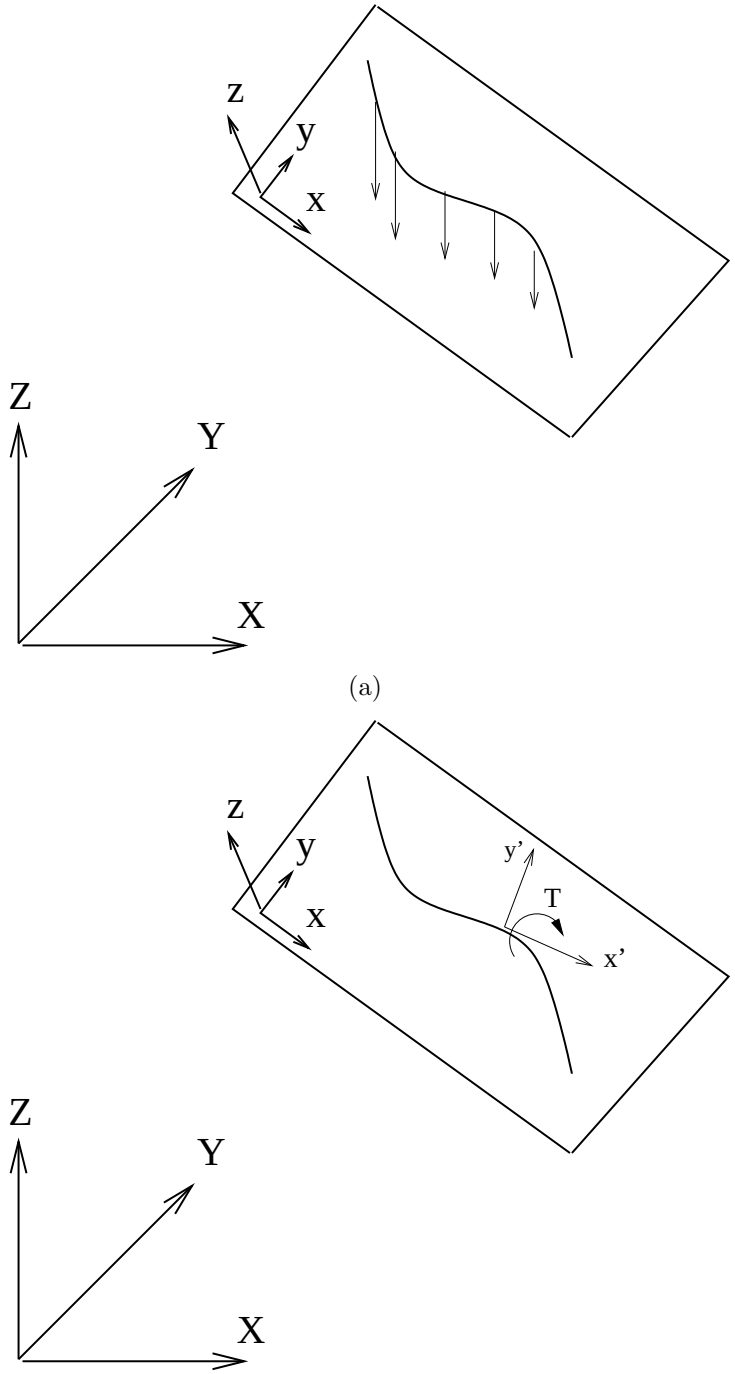

Figure 19: This figure depicts the application of initial perturbations to the salamander model. Figure *a* depicts the application of initial forces on the links in -ve *Z* direction. Figure *b* depicts the application of initial torques on the links about the direction of their body axis i.e x' axis.

3-dimensional motion to the salamander model, the model was subjected to two different schemes of force application, one incorporating the application of only inertial forces and the other including application of both inertial as well as viscous forces.

Having understood the procedure used for simulating the motion of model in 3-D, we can now proceed to the analysis of motion of the model upon the application of forces according to two schemes of forces used for analysis in 2-D in Section 4.1 and Section 4.3.1.

6.1 Application of inertial forces to the model

For calculating inertial forces, the basic formulation remains the same as in Section 4.1, only addition being the inertial force in z'-direction of the body coordinate frame of links.

$$F_{i,\parallel} = \lambda_{i,\parallel} v_{i,\parallel}^2 \tag{21}$$

$$F_{i,\perp y'} = \lambda_{i,\perp y'} v_{i,\perp y'}^2 \tag{22}$$

$$F_{i,\perp z'} = \lambda_{i,\perp z'} v_{i,\perp z'}^2 \tag{23}$$

where

$$\lambda_{i,\parallel} = \frac{1}{2} C_{i,\parallel} S_i \rho \tag{24}$$

$$\lambda_{i,\perp y'} = \frac{1}{2} C_{i,\perp y'} S_i \rho \tag{25}$$

$$\lambda_{i,\perp z'} = \frac{1}{2} C_{i,\perp z'} S_i \rho \tag{26}$$

$v_{i,\parallel}$, $v_{i,\perp y'}$ and $v_{i,\perp z'}$are the components of velocity of link i relative to water. The force structure is same as that in Section 4.1, only difference being that in this case force in the direction of z'-axis of the body coordinate frame (refer to Figure 2) attached to the links also becomes significant as motion of the model takes place in 3-D. $\lambda_{i,\parallel}$, $\lambda_{i,\perp y'}$ and $\lambda_{i,\perp z'}$ are drag coefficients identical to the ones discussed in Section 4.1 of this report. The shape of link used for calculating the drag coefficients was that of a cuboid of the dimensions of a body link. For calculating $\lambda_{i,\perp y'}$, the value for S_i was area of the cuboidal face whose normal was in y' direction. Similarly, we calculated $\lambda_{i,\perp z'}$ using the area of cuboidal face whose normal was in z' direction.

Table 4 suggests the parameters used for simulating the swimming motion of salamander model in 3-D.

The parameters for travelling wave superimposed on the model were kept the same as that for 2-D case. The scheme for generating the motion of

salamander model in 3-D is described for the two kinds of perturbations mentioned earlier in this section.

6.1.1 Translational Perturbations

The scheme for applying translational perturbations was as following:

1. Application of initial force of -0.1 N for 5 seconds, on the links in the -ve Z-direction (refer to Figure 2). These initial forces were meant to impart an initial translational acceleration to the model in -ve Z-direction.

2. Determination of components of velocity of the links in global coordinate frame i.e X-Y-Z frame (refer to Figure 2).

3. Transformation of velocity obtained in step 2 to coordinate frame linked to the body of links i.e x'-y' frame (refer to Figure 2).

4. Calculation of inertial forces acting on the links (using Equations 21, 22 and 23).

5. Applying forces to respective links in their body coordinate frames using the functions provided by *ODE* software.

6. Determination of velocity of links and repetition of steps 3, 4 and 5.

Figure 20 depicts a plot of variation in V_Z, i.e the component of velocity of center of mass of the model in global Z-direction. This plot shows that the magnitude of V_Z increases under the influence of initial forces and then attains a terminal velocity. After the forces are removed, the magnitude of V_Z starts decreasing and the rate of this decrease can be used as a basis to compare the influence of various drag forces on the motion of model which we will be doing in this report once we analyse the results for schemes involving viscous forces as well.

6.1.2 Rotational Perturbations

The scheme for applying rotational perturbations was as following:

1. Application of initial torques of -0.001 Nm for 5 seconds, on the links about the x'-direction (refer to Figure 2). These initial torques were meant to impart an initial rotational acceleration to the links about their body axis i.e x' axis.

Link i	$\lambda_{i,\parallel}$ (kg/m)	$\lambda_{i,\perp y'}$ (kg/m)	$\lambda_{i,\perp z'}$ (kg/m)
1	0.3	1.925	1.225
2	0.2	1.925	1.225
3	0.1	1.925	1.225
4	0.0	1.925	1.225
5	0.0	1.925	1.225
6	0.0	1.925	1.225
7	0.0	1.925	1.225
8	0.0	1.925	1.225
9	0.0	1.925	1.225
10	0.0	1.925	1.225

Table 4: Parameters for mechanical simulation of the swimming motion of salamander model in 3-D. Column 1 identifies the link for which coefficients are mentioned in the same row. Column 2 gives the value of parallel drag coefficient whereas Column 3 and Column 4 mention the perpendicular drag coefficients for corresponding link.

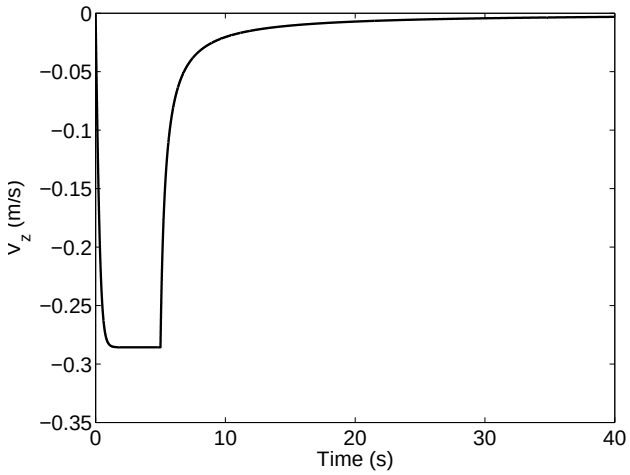

Figure 20: Plot for V_Z, i.e the component of velocity of the model in global Z-direction. It signifies the rate of downward motion of model under the influence of initial downward forces on the body links.

2. Determination of components of velocity of the links in global coordinate frame i.e X-Y-Z frame (refer to Figure 2).

3. Transformation of velocity obtained in step 2 to the coordinate frame linked to the body of links i.e x'-y' frame (refer to Figure 2).

4. Calculation of inertial forces acting on the links (using Equations 21, 22 and 23).

5. Applying forces to respective links in their body coordinate frames using the functions provided by *ODE* software.

6. Determination of velocity of links and repetition of steps 3, 4 and 5.

This analysis was performed with the motive of analysing the angular velocity of plane in which the model swims, about the longitudinal direction of motion of the model. The longitudinal direction was obtained by the scheme illustarted in Section 4.1. Rather than analysing angular velocity of all the links, we chose to perform the analysis for one of the links as all the links were connected by hinge joints, with the hinge axes in direction of normal to the plane in question. So the analysis of rotational motion of one link can convey the required information about rotation of the plane of swimming of the model. We chose the angular velocity of link 5 (ω_5) as the basis of our analysis. The angular velocity was obtained for link 5, in the global coordinate frame with the help of function provided by *ODE* software. The component of angular velocity ($\omega_{x,5}$) in the longitudinal direction i.e x-direction (refer to Figure 2) was obtained by the use of Equation 1.

Figure 21 depicts $\omega_{x,5}$, i.e the component of angular velocity of the body link 5 about the longitudinal direction of motion of the model. The plot depicts that angular velocity of the plane increases in the beginning under the influence of initial torque on the links but starts to decrease as soon as the torque is withdrawn. This decrease can be attributed to the inertial drag acting on the model. As was mentioned in the case of translational perturbations, it will be an interesting proposition to analyse and compare the rotation rates for other force schemes.

6.2 Incorporation of viscous forces in the analysis

In this section, we study the motion of model subject to simultaneous application of both inertial as well as viscous forces. For computation of viscous forces, we adhered to the linear model of viscous forces presented in Section 4.3.1 with the formulation being:

$$F_v = \tau A \approx \mu(V/\delta)A \tag{27}$$

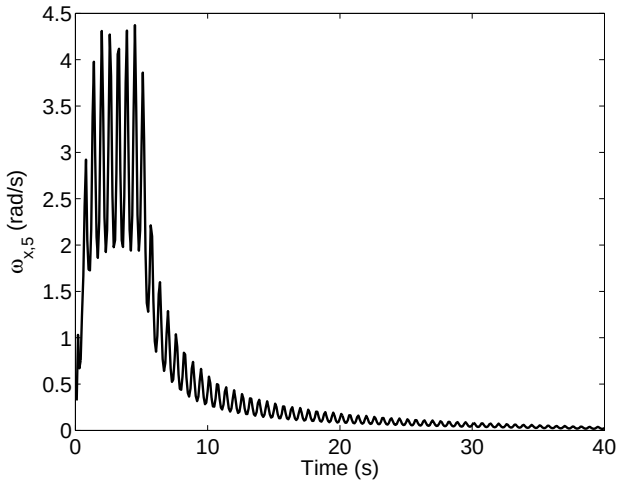

Figure 21: Plot for $\omega_{x,5}$, i.e the component of angular velocity of body link 5 in longitudinal direction. It signifies the rate of rotation of plane of swimming of the model under the influence of initial torques on the body links.

Equation 27 was used to calculate the viscous forces in all the three axis directions of the body coordinate frame attached to the links. Viscous forces so computed were applied to the model along with inertial forces computed according to the formulations presented in Section 6.1 and subsequent motion of the model was observed.

Figure 22 depicts the influence of initial downward forces on the model subjected to both inertial and viscous forces. We find that the plot is similar to that obtained in the previous case involving only inertial forces (refer to Figure 20).

Figure 23 depicts $\omega_{x,5}$, i.e the angular velocity component of the body link 5 about the longitudinal direction of motion of the model and the model was subjected to both inertial as well as viscous forces. The plot depicts that $\omega_{x,5}$ obtained using this force scheme had the same profile as that obtained for the inertial force scheme discussed in Section 6.1. In next section, we will make a comparative analysis of the results obtained for the two forces schemes discussed in Sections 6.1 and 6.2.

6.3 Comparison of results obatined for the two force schemes

The motive of applying initial perturbations to the model was to ascertain the influence of external forces and torques on the model. We used different

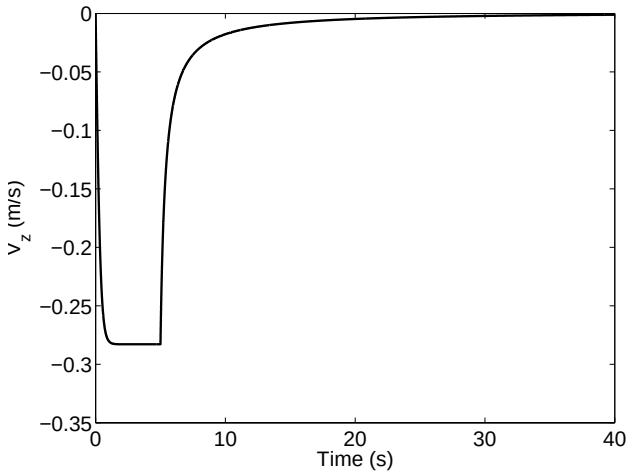

Figure 22: Plot for V_Z, i.e the component of velocity of the model in global Z-direction. This plot was obtained for the scheme in which the model was subject to both inertial as well as viscous forces. It signifies the rate of downward motion of model under the influence of initial downward forces on the body links.

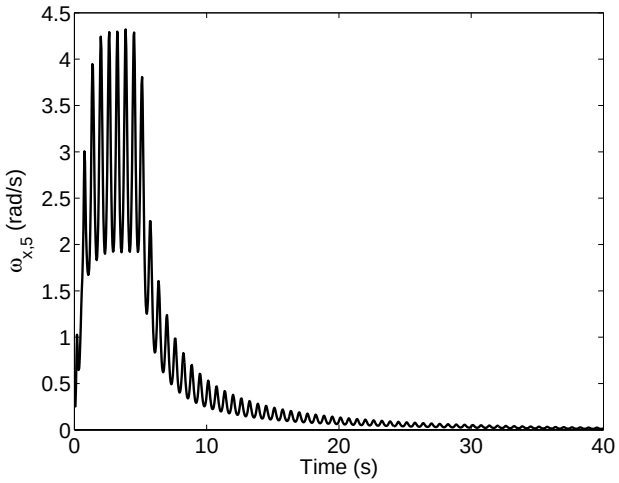

Figure 23: Plot for $\omega_{x,5}$, i.e the component of angular velocity of body link 5 in longitudinal direction. This plot was obtained for the scheme in which the model was subjected to inertial as well as viscous forces. It signifies the rate of rotation of plane of swimming of the model under the influence of initial torques on the body links.

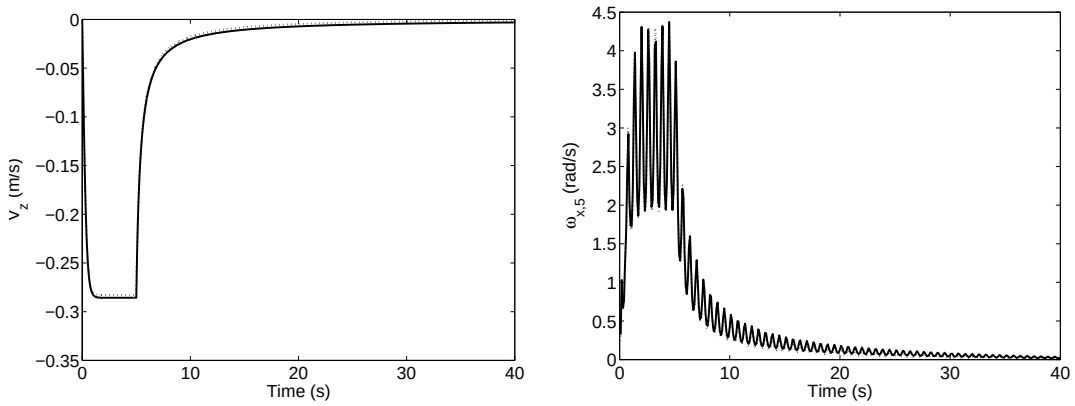

(a) (b)

Figure 24: Figure a presents a comparison between the values obtained for V_Z for two force schemes discussed in the previous two sections. The solid curve represents the plot for inertial scheme whereas dotted curve presents the plot for the scheme involving inertial as well as viscous forces. Figure b presents a comparison between the values obtained for $\omega_{x,5}$ for two force schemes. The solid curve represents the plot for inertial scheme whereas dotted curve presents the plot for scheme involving inertial as well as viscous forces.

force schemes to find out the extent to which various force schemes resist the influence of external perturbations on the motion of model. Figures 24(a) and 24(b) depict the comparison between the results obtained for two schemes used in Sections 6.1 and 6.2. Both the figures indicate that plots obtained for the two schemes almost coincide indicating that the addition of viscous forces in second scheme did not bring about much change in the results obtained. However, we need the help of results of experimentations on a salamander robot to ascertain if it is inertial forces which hold the key to movement of the salamander model at high swimming speeds.

6.4 Demonstration of swimming motion of the model in 3-D

Figure 25 demonstrates swimming motion of the model when forces were applied on the links in 3-D. The figure helps in sustaining the concept of planar swimming. The motion of salamander model as shown in Figure 25, can be considered as a plane which is moving in a particular direction. This plane signifies the motion of center of mass of the model with the aforementioned direction being the longitudinal direction of motion of the model.

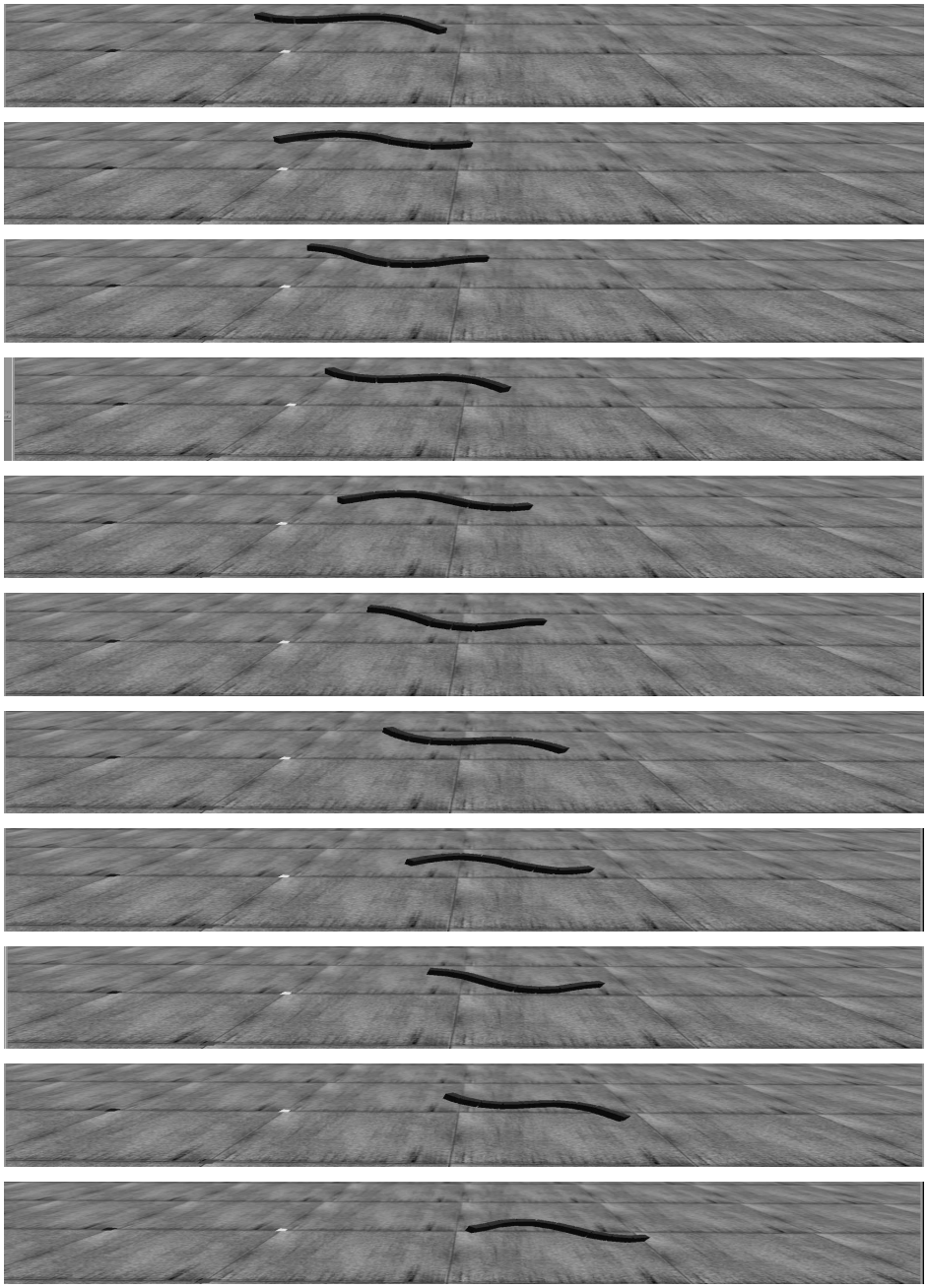

Figure 25: Mechanical simulation of swimming of the salamander model in 3-D. Successive snaps of motion of the model highlight a direction along which the model progressed with time. This direction is the longitudinal direction of motion of the model.

7 Analysis of swimming motion of the legged salamander model

Having analysed the motion of a snake i.e.non-legged model of the salamander in previous sections, we considered it important to analyse the influence of presence of limbs on the motion of salamander model. The necessity of this analysis arose from the fact that the design proposed for construction of the robot which could emulate the swimming motion of a biological salamander, possessed limbs. The code for legged model was developed by Simon Capern, an undergraduate student at EPFL as a part of his semester project and I analysed the influence of hydrodynamic forces on the model generated by his code.

The body framework of salamander model was same as that described in Section 2 with the exception of four limbs which were added to the body of salamander model. Each of these limbs had a construction which consisted of three capped cylinders of dimensions indicated in the Table 5. A capped cylinder is a cylinder with hemispherical end faces. A pair of these limbs was attached to body links 3 and 8 respectively, by one degree of freedom hinge joint with hinge axis set in the direction of local y' axis of the body links described in Section 4.1. These legs were special in the sense that they had the attributes of both limbs as well as wheels.

Cylinder i	Radius(r_i) (m)	Length(l_i) (m)
1	0.015	0.06
2	0.015	0.04
3	0.021	0.001

Table 5: Dimensions for capped cylinders which constituted the limbs of legged model. Column 1 identifies the cylinder number and the subsequent columns provide dimensions of that cylinder.

To describe the relative orientation of three capped cylinders in a limb structure, capped cylinder1 was linked on one longitudinal end, to a body link by one degree of freedom hinge joint and was linked to cylinder 2 by one degree of freedom hinge joint on other longitudinal end. Capped cylinder 2 was linked to cylinders 1 and 3 on its longitudinal ends by one degree of freedom hinge joints. Capped cylinder 3 was free at one end. In our analysis, all hinge joints described above except the joint of Cylinder 1 with the body link, were locked. The orientation and structure of the limbs was as shown in Figure 26. This structure and orientation was in accordance with the design

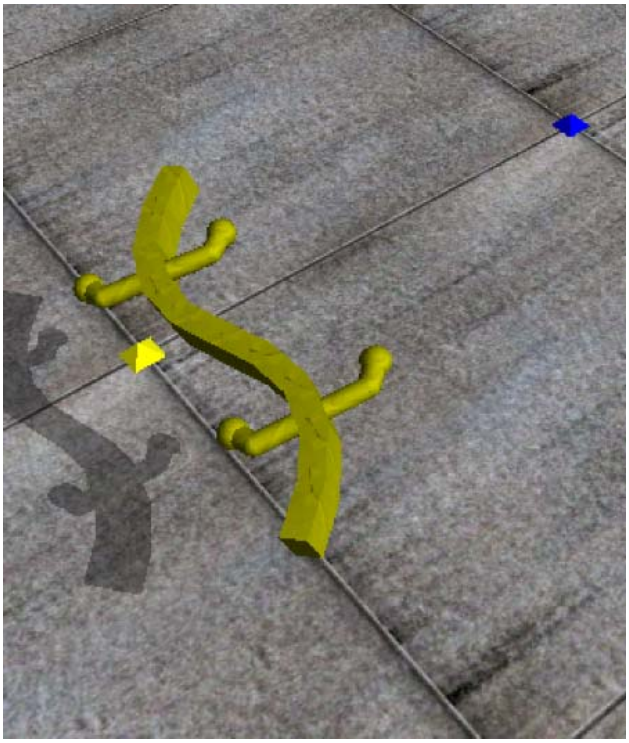

Figure 26: This figure depicts the structure of limbs along with the relative orientation of three capped cylinders in the configuration of limbs.

proposed for construction of the salamander robot, mentioned earlier in this section.

Having fixed the structure and orientation of limbs, we analysed the influence of limbs on various aspects of motion of the salamander model. The attributes of travelling wave superimposed on the model were the same as described in Section 4.1 of the report.

7.1 Influence of limbs on the speed of salamander model.

We applied the inertial force scheme described in Section 4.1 as the basis of comparative analysis between the motion of snake and legged salamander model. The need to analyse the influence of size of limbs on the motion of model motivated us to compute the velocity of model for four sets of values of drag coefficients for the limbs corresponding to limbs of different radii, described in Table 6.

The methods of computation and application of inertial forces to the legged salamander model were the same as that described in Section 4.1.

Intuitively the speed of center of mass of the model was bound to decrease with the addition of greater inertia to the snake model in form of limbs, accompanied by an increase in inertial drag encountered by the model due to the presence of limbs. It was however, an interesting proposition to find out the influence of limbs on the speed of salamander model. Figures 27(a), 27(b), 27(c) and 27(d) give velocity plots for the four sets of values of drag coefficients for the limbs, presented in Table 6.

The mean value of longitudinal component of velocity for four schemes of drag coefficients has been presented in Table 7. It can be easily noticed in Table 7 that the lowest value of mean longitudinal speed was obtained for scheme suggesting the largest value for drag coefficients among all the proposed schemes for drag coefficients. There was a great difference between the values obtained for different schemes suggesting the fact that the structure and orientation of the limbs can play a crucial role in determining the swimming speed of salamander model. It was an interesting proposition to compare variations in the longitudinal speeds for the legged model with the plot obtained for longitudinal speed of the snake model, presented in Section 4.1 of the report.

Figure 28 clearly depicts the influence of presence of limbs on the motion of salamander model. The mean longitudinal speed of the legged model for different values of drag coefficients was considerably lesser than that for the snake model. For the legged model, the schemes with lower values of drag coefficients resulted into a higher value of mean longitudinal speed as compared to schemes proposing a higher value of drag coefficients. Since the drag coefficients are also dependent upon the orientation of limbs relative to the flow of surrounding fluid, the figure suggests that the orientation of limbs should be the one resulting into lesser values of drag coefficients and hence, lesser drag encountered by the model during its motion.

Scheme i	$\lambda_{i,\parallel}$ (kg/m)	$\lambda_{i,\perp y'}$ (kg/m)	$\lambda_{i,\perp z'}$ (kg/m)
1	0.04	0.1	0.1
2	0.1	0.3	0.3
3	0.2	0.6	0.6
4	0.353	0.9	0.9

Table 6: This table presents four schemes representing drag coefficients for the limbs. Column 1 identifies the scheme for which coefficients are mentioned in the same row. Column 2 gives the value of parallel drag coefficient of a limb whereas Column 3 and Column 4 mention perpendicular drag coefficients for the limb.

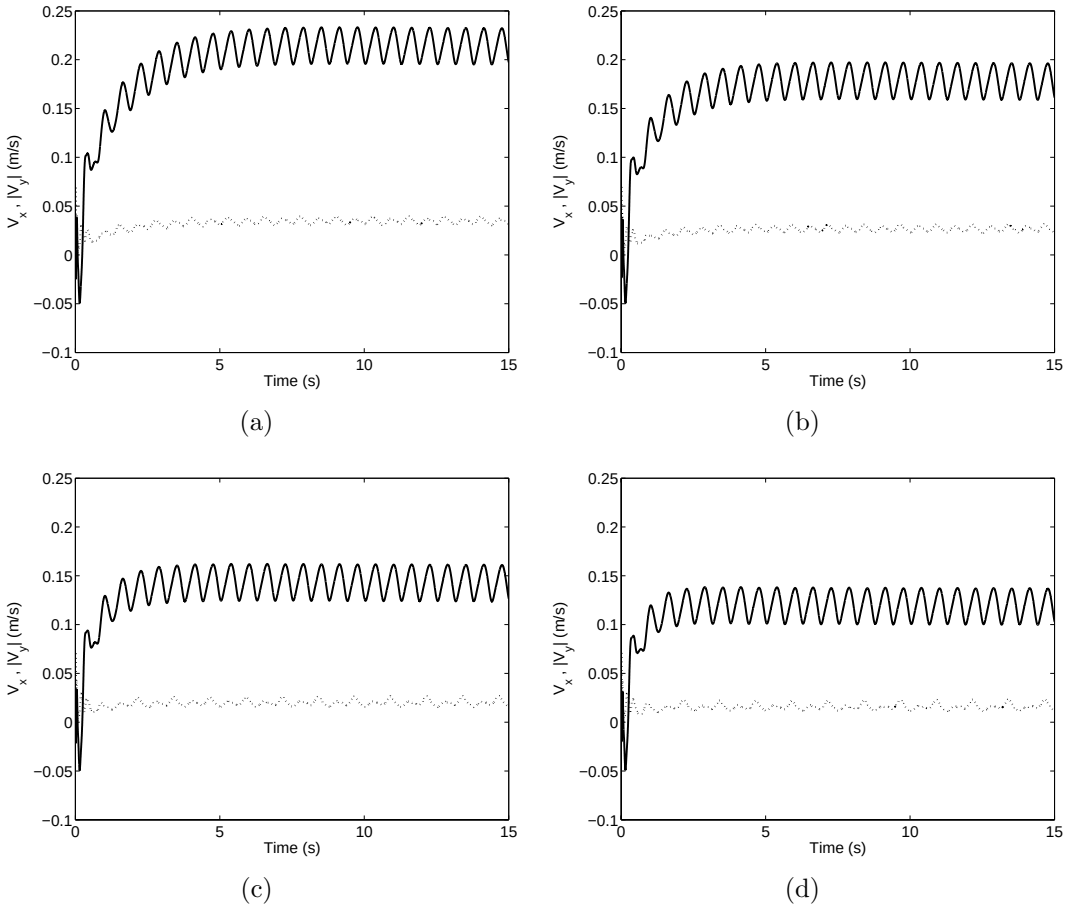

Figure 27: Plots of components of velocity of the legged salamander model when only inertial forces were applied to the model. The velocity plots in this figure represent the results obtained for the schemes of drag coefficients mentioned in Table 6. Figures a, b, c and d show the results obatined for Scheme 1, 2, 3 and 4 respectively, of the drag coefficients mentioned in Table 6. The solid curve represents the longitudinal component of velocity of center of mass of the model and dotted curve represents the magnitude of component of velocity in the lateral direction. x-y axis represent the longitudinal and lateral direction respectively of motion of the model, hence the longitudinal component of velocity has been represented as V_x and the lateral component of velocity has been represented as V_y.

Scheme i	$V_{x,mean}$ (m/s)
1	0.2064
2	0.1729
3	0.1399
4	0.1182
Snake model	0.2394

Table 7: Mean value of the longitudinal component of velocity for four schemes of drag coefficients and for the snake model. Column 1 identifies the scheme of drag coefficients (refer to Table 6) and Column 2 mentions the value of $V_{x,mean}$.

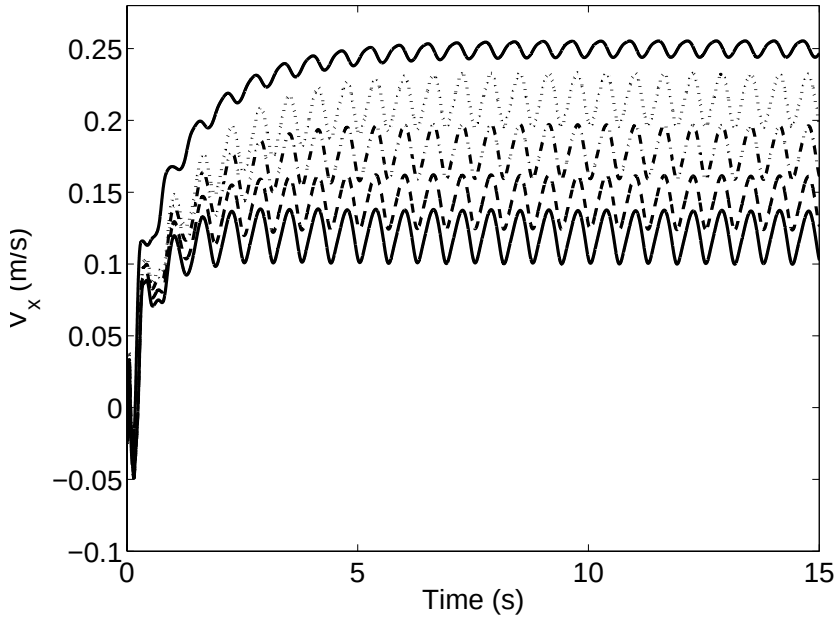

Figure 28: This figure presents a comparison between plots of the longitudinal component of velocity of the snake and legged model of the salamander. The solid curve represents the longitudinal component of velocity of the snake model for the scheme in which only inertial forces were applied to the model. The dotted curve lies below the solid curve and it corresponds to the longitudinal speed of the legged model for the 1^{st} set of values of drag coefficients mentioned in Table 6. The dash-dot curve corresponds to the longitudinal speed of the legged model for the 2^{nd} set of values of drag coefficients and this curve lies below the the dotted curve. Below this curve, is the dashed curve which represents the results obtained for Scheme 3 of the drag coefficients. Finally, there is a solid curve below all the other curves and it denotes the longitudinal velocity for Scheme 4 of the drag coefficients.

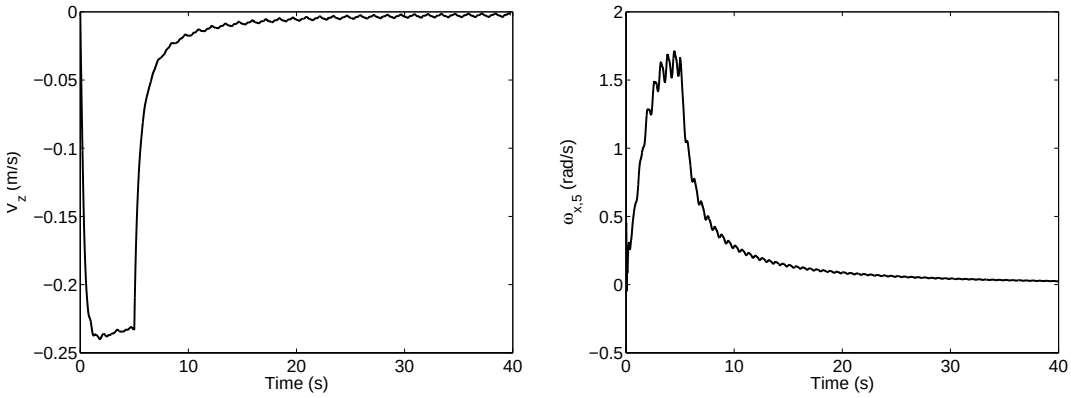

(a) (b)

Figure 29: Figure *a* represents the plot for V_Z, i.e the component of velocity of legged model in global Z-direction. It signifies the rate of downward motion of model under the influence of initial downward forces on the body links. Figure *b* depicts the plot for $\omega_{x,5}$, i.e the component of angular velocity of body link 5 in longitudinal direction. It signifies the rate of rotation of plane of swimming of the model under the influence of initial torques on the body links.

7.2 Influence of limbs on the resistance of salamander model to external perturbations

This analysis was motivated by the analysis done for the snake model in which the snake model was subjected to initial forces and torques to trigger the motion of model in 3^{rd} dimension(refer to Section 6). We were motivated to analyse the motion of legged model under the influence of applied forces and moments, to ascertain if the limbs play any role in determining the motion of salamander model under such initial conditions. The applied forces and moments were of the same nature as described in Section 6 and the motion of legged model was studied to compare the results for legged model with those obtained for the snake model.

Figure 29(a) depicts the plot for Z-component of velocity of the legged model when subjected to initial downward forces. Figure 29(b) shows the plot for angular velocity of swimming plane of the model about the longitudinal direction of motion, when subjected to initial torques about the body axis of links. These figures do not convey a great deal of information about the influence of limbs on the translational and rotational stability of the model. The influence of limbs, will perhaps be evident from Figures 30(a) and 30(b) in which we compare the results for legged model with that obtained for the snake model when subjected to similar external disturbances. Figure 30(a)

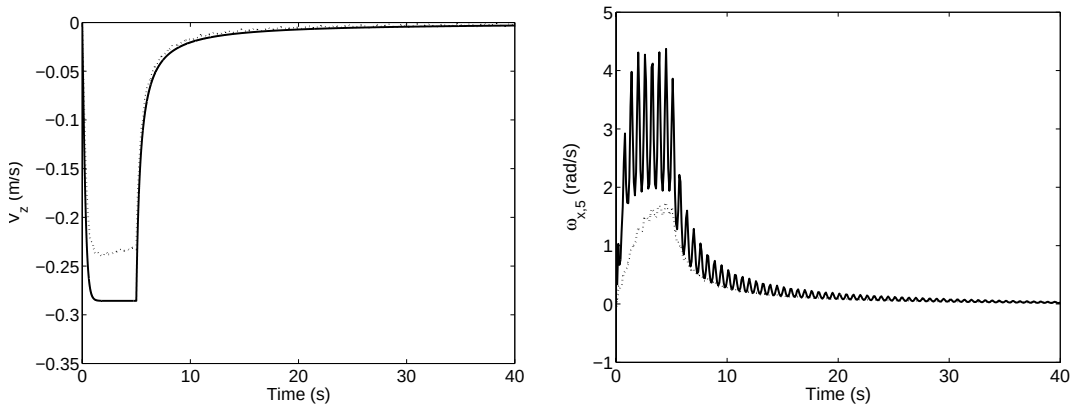

(a) (b)

Figure 30: Figure a presents a comparison between the values obtained for V_Z for the snake and legged model. The solid curve represents the plot for snake model whereas dotted curve presents the plot for legged model. Figure b presents a comparison between the values obtained for $\omega_{x,5}$ for the snake and legged model. The solid curve represents the plot for snake model whereas dotted curve presents the plot for legged model.

shows that the maximum value of V_Z for a legged model is lesser than that attained for a snake model. Similarly, Figure 30(b) shows that the legged model attains a lower value of $\omega_{x,5}$ as compared to that obtained for a snake model. These plots therefore, qualitatively present the view that the presence of limbs improves the stability of salamander model. However, these plots may not be representing the exact difference between the behaviour of snake and legged salamander model under the influence of external perturbations. Experimentations on a salamander robot will bring out the difference between the behavour of snake and legged salamander model.

8 Acknowledgements

I am thankful to Prof. Auke Jan Ijspeert for the invaluable guidance given by him to me during the course of this Project. I gratefully acknowledge the contributions made by Alessandro Crespi and Jonas Buchli in the implementation of this Project. I am thankful to Alessandro Crespi and Simon Capern for developing the code for simulation of the salamander model. I am also grateful to the Logic Systems Laboratory, EPFL for making my stay and project work in Switzerland a memorable one.

References

[1] Ö. Ekeberg. A combined neuronal and mechanical model of fish swimming. *Biological Cybernetics*, 69:363–374, 1993.

[2] A.J. Ijspeert. A connectionist central pattern generator for the aquatic and terrestrial gaits of a simulated salamander. *Biological Cybernetics*, 84:331–348, 2001.

[3] K. Muralidhar and G. Biswas. *Advanced Engineering Fluid Mechanics*. Narosa Publishing House, 1996.